Geological Society of America
Special Paper 374
2003

Geothermal gradients in continental magmatic arcs: Constraints from the eastern Peninsular Ranges batholith, Baja California, México

David A. Rothstein*
Craig E. Manning
Department of Earth and Space Sciences, University of California, Los Angeles, California 90095-1567, USA

ABSTRACT

In continental arcs the extension of geothermal gradients derived from shallow crustal levels to depth predicts widespread melting at pressures that are inconsistent with seismic studies. Numerical models of low-pressure metamorphism in continental arcs suggest that these extrapolations are problematic because magmatic advection is the dominant mechanism of heat transport in these terranes rather than conduction from the base of the lithosphere. Metamorphic thermobarometry data from the middle crust of the eastern Peninsular Ranges batholith in Baja California, México, provide a useful field test of these models. Graphite-bearing pelitic and semi-pelitic schists record peak metamorphic temperatures of 475–720 °C at pressures of 3–6 kbar. These data bridge a gap between shallow and deep crustal levels of continental magmatic arcs in the southwestern United States and Baja California, México. Recognition of the transient, isobaric heating that accompanies contact metamorphism allows the definition of a gradient in minimum wall-rock temperatures of ~22 °C/km from 10 to 25 km with thermobarometric data from the eastern Peninsular Ranges batholith and other continental arcs that have relatively simple thermal histories. This gradient defines a maximum background geotherm that reconciles the results of geophysical and numerical models with wall-rock thermobarometry and is consistent with the formation of granulites in the lower crust of sub-arc regions and numerical models of the thermal effects of nested plutons. Recognition of the proposed geotherm may lower estimates of the depth to the seismic Moho and increase strain and unroofing rates inferred from structural and thermochronologic studies, respectively.

Keywords: geothermal gradients, continental arc, contact metamorphism.

INTRODUCTION

The thermal structure of the crust plays a central role in the geophysical, geologic, geochemical, and isotopic evolution of continental magmatic arcs. Because rheology is sensitive to temperature, the distribution of heat in continental arcs affects seismic velocities and strain partitioning (Birch, 1961; Christensen, 1982; Christensen and Fountain, 1975; Furlong and Fountain, 1986; Paterson and Tobisch, 1992). The distribution of thermal energy also influences crustal melting (e.g., Wyllie, 1979). Cooling histories derived from mineral thermochronometers are also sensitive to assumptions about temperature changes during cooling (e.g., McDougall and Harrison, 1988).

Understanding the thermal evolution of continental arcs requires quantitative observational constraints on changes in

* Present address: DRP Consulting, Inc., 2825 Wilderness Place, Suite 1000, Boulder, Colorado 80301, USA.

Rothstein, D.A., and Manning, C.E., 2003, Geothermal gradients in continental magmatic arcs: Constraints from the eastern Peninsular Ranges batholith, Baja California, México, *in* Johnson, S.E., Paterson, S.R., Fletcher, J.M., Girty, G.H., Kimbrough, D.L., and Martín-Barajas, A., eds., Tectonic evolution of northwestern México and the southwestern USA: Boulder, Colorado, Geological Society of America Special Paper 374, p. 337–354.

temperature with depth across a broad range of crustal levels. Hereafter we refer to these depth-dependent variations in temperature as geothermal gradients or geotherms without implying specific conditions regarding basal heat fluxes, thermal conductivity, or surface heat flow. In continental arcs geothermal gradients are relatively well understood to depths of 10–15 km from surface heat flow data and metamorphic petrology (Table 1), whereas geotherms in the middle and deep crust are poorly known. The absence of well-studied examples of deeper crustal levels of magmatic arcs requires extending geothermal gradients inferred from shallow depths to higher pressure. However, seismic velocity and other geophysical studies indicate that the inferred geotherms do not extrapolate sensibly to the deeper crust (e.g., Giese, 1994). Accounting for the temperature and pressure dependence of thermal conductivity, surface heat-flow values of 90 mW/m^2 measured in the Andes extrapolate to >1400 °C at 35 km (Arndt et al., 1997), which exceeds the basalt liquidus (e.g., Yoder and Tilley, 1962; Thompson, 1972). If melt is present in the central Andean crust, it constitutes less than 20% of the volume (Schilling and Partzsch, 2001). Heating to solidus temperatures at >25 km in the Cascades would yield higher inland heat flow than is currently observed (Morgan, 1984).

These observations require that geothermal gradients change in the middle crust of active continental arcs. In this paper, we exploit exposures of the middle crust in the eastern Peninsular Ranges batholith in Baja California, México, (Rothstein, 1997) to constrain the nature of this change and the range of possible background geothermal gradients that attend the middle crust during arc magmatism. The paper begins by reviewing observations that constrain geothermal gradients in continental arcs. We then describe a conceptual framework for using wall-rock thermobarometry to constrain the background geothermal gradient in continental magmatic arcs. A description of the geologic setting and metamorphism of the eastern Peninsular Ranges batholith in Baja California México follows. We combine these results with pressure-temperature (P-T) data from other relatively simple continental arcs to bridge the gap in data between the upper and lower crust of these terranes. We then use two-dimensional numerical models to investigate the validity of the proposed mid-crustal geothermal gradient and conclude by discussing the geotherm's implications for seismic velocity, structural, and thermochronologic data from continental arc terranes.

OBSERVATIONS FROM CONTINENTAL ARCS

Geothermal gradients have been derived from surface heat flow for two well-studied, active continental arcs, the Andean and Cascade ranges. Heat flow in these systems is low in the outer arc region (~40 mW/m^2), high in the active arc and backarc (>80 mW/m^2), and low toward the stable craton (~40 mW/m^2; Uyeda and Watanabee, 1982; Giese, 1994; Henry and Pollack, 1988; Springer and Förster, 1998). Modeled geothermal gradients for the active portions of these arcs range from 30 to 35 °C/km in the upper 35 km (Morgan, 1984; Giese, 1994) to ~50 °C/km in the upper 12 km (Henry and Pollack, 1988). Surface heat-flow in other active arcs can range to higher values (e.g., Gill, 1981; Furukawa and Uyeda, 1989), which requires even higher geothermal gradients.

Studies of shallow crustal levels exhumed from ancient magmatic arcs show that variations in peak metamorphic temperatures at low pressures broadly agree with geothermal gradients inferred from surface heat flow. The metamorphic belts associated with those terranes are typically exhumed from ≤15 km, where P-T-t paths imply rapid, nearly isobaric metamorphism with metamorphic field gradients of 35–150 °C/km (e.g., Barton et al., 1988; De Yoreo et al., 1991). Gradients significantly exceeding the 35–50 °C/km suggested by surface heat flow can plausibly be explained by local, transient heating events during contact metamorphism, which produce peak metamorphic temperatures that do not reflect a background crustal geotherm (Barton et al., 1988)

Estimates of geothermal gradients from both heat-flow and metamorphic data are subject to significant uncertainty. For

TABLE 1. GEOTHERMAL GRADIENTS IN MAGMATIC ARCS

Data/method	Geothermal gradient	Source
Cascade Arc heat flow Transition zone half widths	45°C/km (0–15 km)	Blackwell et al. (1982) Blackwell et al. (1990)
Andean and Cascade heat flow Transition zone half widths	25–30°C/km (0–25 km); <20°C/km below 25 km	Morgan (1984)
Basaltic underplating/numerical models	~30°C/km (0–25 km) ~17°C/km (25–40 km)	Wells (1980)
Regional granitic sill emplacement/numerical models	~35°C/km (0–25 km) ~10°C/km (25–50 km)	Wells (1980) Lux et al. (1985)
Multiple diapirism/numerical models	~45°C/km (0–10 km) 15–18°C/km (10–30 km)	Barton and Hanson (1989)
Metamorphic field gradients	~50°C/km (0–15 km)	Turner (1981)
Granulite thermobarometry	30–35°C/km (0–25 km)	Bohlen (1991)
Melt-residue xenolith thermobarometry	~20°C/km (0–40 km)	Miller et al. (1992)

example, hydrothermal effects (e.g., Blackwell et al., 1982, 1990; Ingebritsen et al., 1989, 1992) and parameter uncertainty and geometric assumptions (Furlong et al., 1991) complicate the interpretation of heat-flow data. Similarly, estimating geothermal gradients from metamorphic P-T-t paths is complicated by the fact that metamorphism is a response to a perturbed geotherm, by uncertainties in regional gradients in the age of peak metamorphic temperatures, and by post-metamorphic shortening or extension (e.g., England and Richardson, 1977; Miller et al., 1992a). But even if these considerations can be addressed adequately, a more important uncertainty arises from the fact that much of the heat in continental arcs may be advected by magma. The thermal histories that result from such heating are very different from those in classical regional metamorphic terranes, where regionally extensive heat sources in the lower crust and upper mantle drive metamorphism (e.g., England and Thompson, 1984).

In magmatic arcs experiencing little tectonically driven disruption of the crust, magmatic advection is the predominant heat transport mechanism that influences temperatures in the upper and middle crust (e.g., Barton and Hanson, 1989; De Yoreo et al., 1991). Numerical models suggest that geothermal gradients in continental arcs are high in the upper crust but decrease significantly below the level at which magmas pond. For example, simple, one-dimensional models of the thermal effects of granitic sills in the middle crust predict high geothermal gradients (~50 °C/km) in the upper 20–25 km of the crust that decrease rapidly to ~15 °C/km between 25–40 km (e.g., Lux et al., 1985; Wells, 1980; Rothstein and Hoisch, 1994). Two-dimensional models accounting for the emplacement of multiple diapiric plutons predict that thermal gradients in the upper 10 km of the crust are high (~35 °C/km) but decrease to ~20 °C/km between 10 and 35 km (Barton and Hanson, 1989; Hanson, 1995). These results indicate that interpretations of geothermal gradients from metamorphic thermobarometers require a conceptual framework that recognizes magmatic advection as the dominant heat transport process in the middle and upper crust of continental arcs.

CONCEPTUAL FRAMEWORK

The numerical models described above make specific predictions about metamorphism in magmatic arcs. Magmas pond and crystallize in the middle and upper crust, liberating heat that drives contact metamorphism. Numerical and analytical models of heat transport, metamorphic mineral assemblages and textures, and mineral thermochronometers consistently show that the high-temperature history of wall rocks is short-lived, on the order of 1–3 m.y. depending on the size of the individual pluton (e.g., Lovering, 1935; Jaeger, 1964; Hanson and Gast, 1967; Krumenacher et al., 1975; Harrison and Clarke, 1979; Joesten and Fisher, 1988; Mahon et al., 1988; Miller et al., 1988; Lovera et al., 1999). The intruded crust experiences localized, contact metamorphism during short-lived events that, when integrated over the history of the construction of the arc, give the appearance of a regionally metamorphosed terrane that was simultaneously at moderate to high temperature (e.g., Barton and Hanson, 1989). However, there is a "background" geothermal gradient that characterizes much of the crust throughout the duration of arc magmatism. At any given time, only a fraction of the crust is at temperatures elevated above this background geotherm, and the timing of these departures varies throughout the terrane. Because the background geotherm is not significantly elevated on a regional scale, the metamorphic field gradient does not reflect the geothermal gradient. If the metamorphic record is inconsistent with these predictions, then alternative models must be considered, such as elevated heat flux from the mantle (e.g., Miyashiro, 1973; Wickham and Oxburgh, 1985, 1987; Bodorokos et al., 2002).

Figure 1 presents a schematic illustration of this conceptual framework. In stable shield lithosphere, there is little lateral variation in temperature within the crust (Condition I, Fig. 2A). The emplacement of plutons in the crust creates thermal perturbations in the wall rocks. The magnitude of the perturbations varies depending on proximity to the pluton. Heating is greatest in the roof pendants above plutons and at sidewall contacts (Condition IV and III, respectively, Fig. 2A) and diminishes with distance from pluton margins (Condition II, Fig. 2A). Because wall rocks adjacent to the tops and sides of a pluton will record increasing peak metamorphic temperatures as the pluton is approached, the minimum wall-rock temperature will represent the smallest excursion from ambient wall-rock temperature during arc magmatism. The locus of these P-T points traces a maximum background geotherm (MBG) that represents the highest possible ambient temperatures at a given depth (Fig. 1B). The actual ambient temperature distribution (Condition II) lies anywhere between the upper limit defined by the MBG and the lower limit defined by a geothermal gradient that was present prior to arc magmatism. We conservatively assume this lower limit to be 18 °C/km, which is broadly characteristic of stable continental lithosphere before the inception of arc magmatism.

Syn- to post-magmatic tectonism will, to varying degrees, drive departures from the idealized thermal structure shown in Figure 1. Cases where terranes have complex polymetamorphic histories, such as the Idaho batholith, United States (Wiswall and Hyndman, 1987; Hyndman and Foster, 1989), the Coast Plutonic Complex of British Columbia, Canada, (e.g., Rusmore and Woodsworth, 1994; Crawford et al., 1987) and deep-seated rocks from the Andean batholith (e.g., Grissom et al., 1991; Kohn et al., 1995; Lucassen and Franz, 1996) were excluded for this reason. Our goal is to focus on continental arc terranes with metamorphic histories that were relatively unaffected by syn- to post-batholithic deformation, such as the eastern Peninsular Ranges batholith.

EASTERN PENINSULAR RANGES BATHOLITH

Geologic Setting

Our study focused on the petrology of wall rocks from the eastern Peninsular Ranges batholith in Baja California Norte,

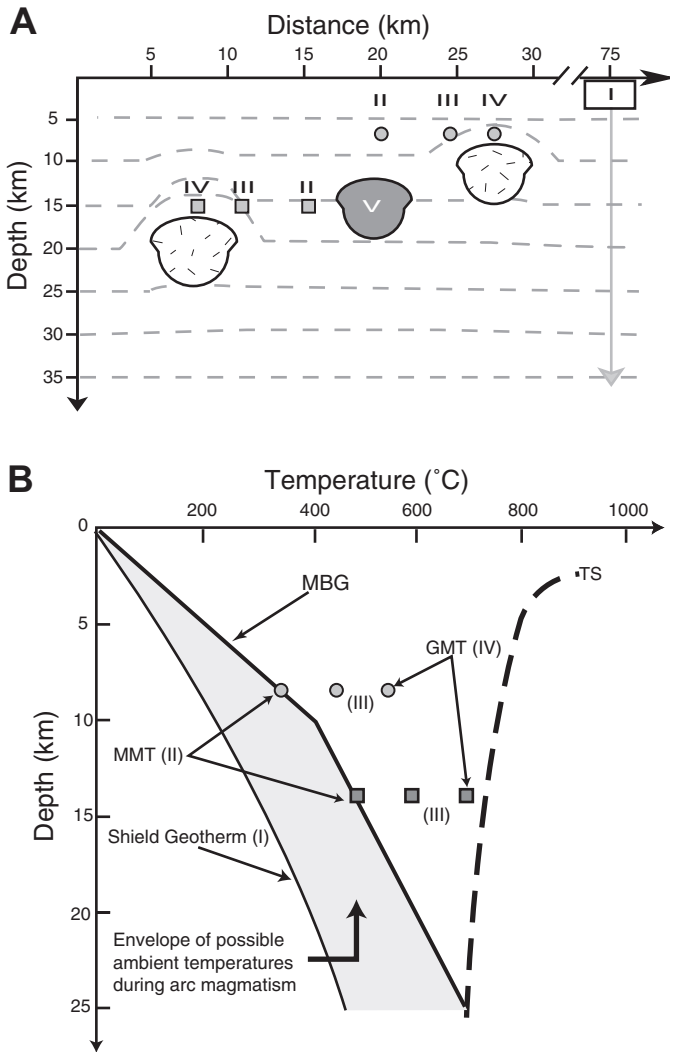

Figure 1. Conceptual model of temperature gradients in continental magmatic arcs. A: Summary of five different temperature conditions that can result during arc magmatism; diagram represents distribution of temperatures at a single time. (I) Continental crust before magmatism; note break in horizontal distance axis. (II) Ambient temperature distribution in between plutons. (III) Temperatures adjacent to side of diapiric pluton. (IV) Temperatures above diapiric plutons. (V) Older pluton that has cooled completely and no longer affects temperatures of adjacent wall rocks. B: Schematic diagram of P-T paths in continental arcs, modified after Lister and Baldwin (1993). Rocks are subjected to thermal effects of emplacement of two plutons at different structural levels. Labels in roman numerals are similar situation to that described for (A). Pluton crystallization isobarically heats wall rocks at two different crustal levels. Greatest metamorphic temperatures (GMT) are recorded by rocks close to igneous contacts (IV), whereas minimum metamorphic temperatures (MMT) are recorded distal to igneous contacts (II). Locus of minimum metamorphic temperatures defines maximum background geotherm (MBG, see text). Actual background temperatures extant during arc magmatism (condition (II) in 2A) are indicated by gray shaded area lying between MBG and shield geotherm (a).

México. The eastern Peninsular Ranges batholith is a fragment of a continental arc that was accreted to the western edge of the North American plate in Jurassic–Cretaceous time. The batholith extends for 1100 km from southern California, USA, to Baja California Sur, México (Fig. 2). Belts of longitudinal consistency and transverse asymmetry occur in prebatholithic lithologies, and in the major element geochemistry, rare earth element signatures, isotopic composition, geochronological signature of plutonic rocks, and grade of wall-rock metamorphism (Gastil et al., 1975; Taylor, 1986; Silver and Chappell, 1988, and references therein; Todd et al., 1988). The transverse asymmetry may result from the juxtaposition of a western island arc terrane against the eastern Peninsular Ranges batholith continental arc at 115–108 Ma (Johnson et al., 1999). The batholithic rocks are predominantly tonalitic to granitic in composition (e.g., Walawender et al., 1990). Available U-Pb zircon measurements and field mapping indicate that >90% of the batholith preserved west of the San Andreas transform was emplaced between 120 and 90 Ma (Silver and Chappell, 1988); the remainder of the batholith consists of earlier Jurassic intrusions (Todd et al., 1991).

Structural, geochronologic, and thermochronometric considerations are important for understanding the metamorphic history of the eastern Peninsular Ranges batholith. Most of the plutons in the eastern Peninsular Ranges batholith were emplaced between ca. 100 and 90 Ma. Mesozoic mylonitic deformation in the Jurassic Cuyamaca–Laguna Mountains Shear Zone and Late Cretaceous Eastern Peninsular Ranges Mylonite Zone involved west-directed thrusting with minor extensional overprinting (e.g., Sharp, 1967; Simpson, 1984; Erskine and Wenk, 1985; Thomson and Girty, 1994). Thermochronologic data from these shear zones indicate that deformation post-dated cooling from temperatures >450 °C ca. 10–30 m.y. after plutonism, such that high-temperature history of the wall rocks was relatively unaffected by deformation (Goodwin and Renne, 1991; Grove, 1993, 1994).

In the Baja California, México, portion of the batholith, thermochronologic data suggest the high temperature portion of the thermal history batholith was relatively unaffected by post-magmatic deformation. Contractional deformation proceeded intermittently from the Late Devonian–Mississippian Antler orogeny to the emplacement of Cretaceous plutons (Gastil and Miller, 1993, and references therein). Biotite K-Ar and $^{40}Ar/^{39}Ar$ apparent ages of 85–80 Ma in the eastern batholith and K-feldspar cooling histories from the northeastern batholith indicate slow cooling after magmatism (Krumenacher et al., 1975; Ortega-Rivera et al., 1997; Rothstein, 1997). A well-developed Eocene erosional surface on the granitic rocks over much of the crest of the Peninsular Ranges, combined with regionally consistent 60–70 Ma apatite fission track results from the central and eastern batholith and stratigraphic constraints suggest ~1 mm/yr unroofing rates throughout much of the batholith between the end of magmatism in Late Cretaceous and Eocene time (Minch, 1979; Dokka, 1984; George and Dokka, 1994). $^{40}Ar/^{39}Ar$ age distributions of detrital K-feldspars in forearc basin strata derived from the northern Peninsular Ranges batholith record closure temperatures from 105 to 75 Ma, which overlap closure ages of basement rocks in

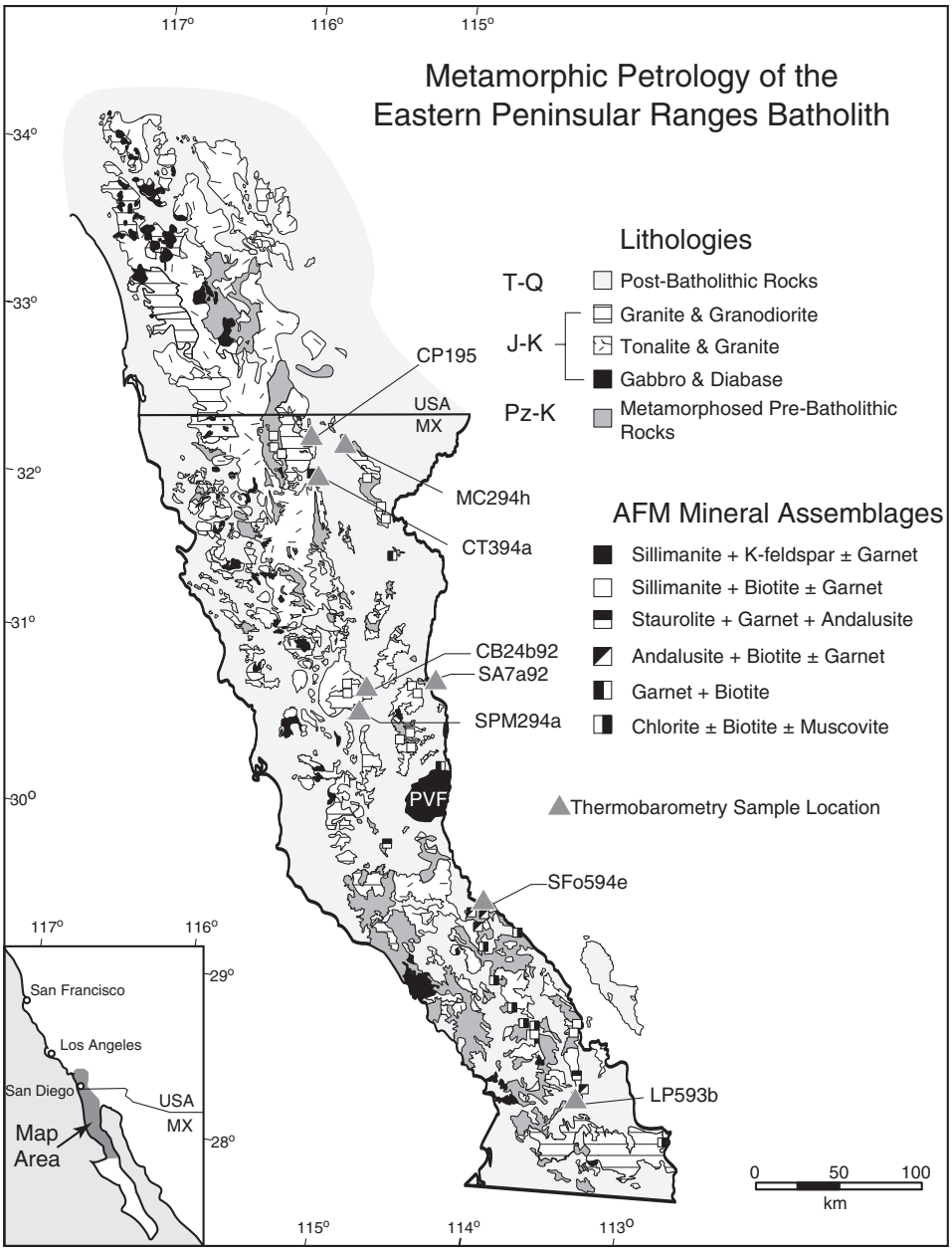

Figure 2. Simplified geologic map of Peninsular Ranges batholith showing observed mineral assemblages and thermobarometry sample locations in eastern Peninsular Ranges batholith. Geology generalized after regional maps from Krumenacher et al. (1975) and Gastil and Miller (1993). PVF—Puertocitos volcanic field.

the eastern Peninsular Ranges batholith (e.g., Lovera et al., 1999). Neogene extensional and strike-slip faulting largely generated the Basin and Range topography of the eastern batholith (Stock and Hodges, 1989) but did not affect the cooling histories of the exposed mid-crustal metamorphic rocks (Rothstein et al., 1995).

Regional Metamorphism in the Eastern Peninsular Ranges Batholith

Both miogeoclinal and slope-basin deposits contain graphite-bearing pelitic and semi-pelitic protoliths (Fig. 2). The predominance of wall rocks with semi-pelitic bulk compositions limits the number of lithologies suitable for thermobarometry. We identified eight metapelite localities for thermobarometry studies. Table 2 summarizes the mineralogy of these rocks. Important index minerals include chlorite in the greenschist facies, garnet ± andalusite ± staurolite in the lower amphibolite facies, and garnet ± sillimanite ± cordierite ± K-feldspar in the upper amphibolite facies. Graphite and ilmenite are ubiquitous accessory phases; apatite, zircon, monazite, and tourmaline are also common. Migmatitic textures are common in the higher-grade rocks. Rothstein (1997) discussed the distribution and composition of mineral assemblages throughout the eastern Peninsular Ranges batholith in Baja California Norte in detail.

TABLE 2. MINERAL ASSEMBLAGES FOR THERMOBAROMETRY SAMPLES

Sample number	Qtz	And	Sil	Grt	Crd	St	Bt	Chl	Ms	Pl	Kfs	Gr	Ilm	Ap	Zrn
MC294h	x		x	5			10–15			30	x	tr	tr	tr	
CP195	x		x	8			20	tr		20	x	tr	tr	tr	tr
CT394a	x		10–15	5–10	<5		30–40			20	x	tr			tr
SA7a92	x		x	3			3	x	5–10			tr	tr	tr	
CB24b92	x		<5	10–15	5–10		50–60	x				tr	tr	tr	tr
SPM294a	x		x	15			40–50	tr		10–20	x	tr	tr		
SFo594e	x	5–10		<5			10–15	x	15–20	5–10		tr	tr	tr	tr
LP593b	x		<3	10			5	x	15	10–15		tr		tr	

Note: Where given, numbers refer to estimated percentage of mode. Mineral abbreviations after Kretz (1983); tr—trace. Sample locations are posted on Figure 2.

Observed textures indicate varying degrees of dynamic recrystallization. Rock matrices are dominated by lepidoblastic muscovite + biotite folia interlayered with granoblastic quartz + plagioclase bands. Garnet, staurolite, cordierite, andalusite, and crystalline, and fibrolitic sillimanite form pre-, syn-, and post-kinematic porphyroblasts in amphibolite facies rocks. Textural evidence does not indicate that there was significant thermal overprinting after peak metamorphism, which is consistent with the thermochronologic database from the region.

Mineral compositions were determined by electron microprobe analysis. Compositions are given in Tables 3–6. Garnets are compositionally homogenous with the exception of steep compositional gradients at the outer 1–3 microns of some grains. Analyses from these regions were excluded from the data used in the thermobarometry calculations. Chlorite is a minor retrograde phase in some rocks, partially replacing biotite, garnet, and staurolite. Rocks with evidence of strong retrogression were excluded from the thermobarometry study.

Thermobarometry

The P-T calculations used TWEEQU software (Berman, 1991). Table 7 summarizes the equilibria used to calculate temperatures and pressures. The temperature calculations employ the Fe-Mg exchange reaction between garnet and biotite. The anorthite breakdown reaction allows the calculation of pressure for six plagioclase-bearing assemblages. Equilibria among garnet, biotite, muscovite, sillimanite, and quartz allow the calculation of pressure for one sample (SA7a92a). Equilibrium between cordierite, garnet, sillimanite, and quartz allows the calculation of pressure for one cordierite-bearing sample (CB24b92). The calculations employ activity models of Berman (1990) for garnet, McMullin et al. (1991) for biotite, and Fuhrman and Lindsley (1988) for feldspar model for plagioclase. An ideal solution model is used for hydrous cordierite.

Sources of errors in metamorphic barometry include the accuracy of the experimentally located end-member reaction, analytical imprecision, uncertainties in microprobe standards and α-factors, thermometer calibration errors, variations in activity models, and compositional heterogeneities (e.g., Kohn and Spear, 1991). Of these, uncertainties in compositional heterogeneities are the most difficult to treat with a global statistical approach. In this study, compositional heterogeneities were considered by performing multiple P-T calculations that accounted for the range of compositions determined for the relevant mineral phases. Rothstein (1997) discussed the details of these calculations.

Figure 3 plots the results of the P-T calculations. Temperatures range from 475 to 720°C at pressures of 3–6 kbars; most of these results fall between the classical Barrovian and Buchan metamorphic field series. The reported P-T estimates and their associated uncertainties are the average and standard deviation (1σ), respectively, of each set of calculations.

Comparison to P-T Data from Other Continental Arcs

Available P-T data from other continental arc settings include heat flow values from active continental arcs and thermobarometric estimates from other studies. Table 8 lists these data and their sources; they were selected from continental arcs where available structural and thermochronologic constraints indicated relatively simple thermal histories dominated by magmatic heating rather than tectonic thickening.

The previously described heat flow data from the Andean and Cascade volcanic arcs indicate a wide range of thermal gradients in the upper crust. Metamorphic thermobarometry data from the middle crust of continental arcs include data from the Sierra Nevada batholith, United States; the Ryoke metamorphic belt, Japan; and the Peninsular Ranges batholith from southern California, United States, and Baja California, México. In the Mesozoic Sierra Nevada batholith, P-T estimates are from thermobarometry or phase relations in contact metamorphic rocks that formed pluton roof pendants (Loomis, 1966; Morgan, 1975; Ferry, 1989; Hanson et al., 1993; Davis and Ferry, 1993). These data indicate high temperatures (~450 °C) at low (2–3 kbar) pressures, consistent with numerical results that predict strong heating directly over crystallizing intrusions. Thermobarometry from pelitic rocks in the Tehachapi Mountains in the southern Sierra Nevada batholith indicate P-T conditions of 620–770 °C at 5.3–6.0 kbar (Dixon et

TABLE 3. AVERAGE GARNET COMPOSITIONS

(avg. of)	MC294h (10)	CP195 (23)	CT594 (15)	SA7a92 (32)	CB24b92 (32)	SPM294a (24)	SFo594e (16)	LP593b (10)
SiO_2	38.58 (0.22)	38.19 (0.21)	38.41 (0.49)	38.92 (0.43)	38.04 ((0.23)	38.19 (0.22)	37.29 (0.43)	38.15 (0.17)
Al_2O_3	21.94 (0.13)	21.84 (0.11)	21.88 (0.30)	21.65 (0.25)	21.68 (0.13)	21.53 (0.18)	21.14 (0.17)	21.71 (0.11)
TiO_2	0.02 (0.02)	0.02 (0.02)	0.02 (0.02)	0.02 (0.02)	0.04 (0.04)	0.04 (0.03)	0.22(0.45)	0.01 (0.01)
Cr_2O_3	0.06 (0.04)	0.05 (0.02)	0.01 (0.02)	0.03 (0.03)	0.04 (0.03)	0.07 (0.04)	0.03 (0.03)	0.04 (0.03)
FeO	32.06 (0.45)	33.94 (0.29)	31.85 (1.66)	28.02 (0.77)	36.76 (0.66)	31.36 (0.30)	25.67 (2.14)	30.28 (0.35)
MnO	1.56 0.53)	2.39 (0.31)	4.63 (0.19)	8.66 (1.70)	0.77 (0.08)	5.12 (0.32)	13.27 (2.42)	8.20 (0.16)
MgO	5.26 (0.81)	3.64 (0.24)	3.73 (0.13)	4.21 (0.85)	3.38 (0.30)	2.98 (0.22)	1.73 (0.26)	2.53 (0.05)
CaO	1.28 (0.06)	1.40 (0.05)	0.87 (0.11)	1.07 (0.19)	0.91 (0.08)	1.97 (0.14)	1.11 (0.22)	0.98 (0.16)
Na_2O								
K_2O								
Total	100.76 (0.38)	101.46 (0.40)	102.03 (0.63)	102.59 (0.90)	101.61 (0.60)	101.26 (0.46)	100.44 (0.41)	101.89 (0.46)
Sum O	12	12	12	12	12	12	12	12
Si	3.02	3.01	3.02	3.03	3.01	3.02	3.01	3.02
Al	2.02	2.03	2.03	1.98	2.02	2.01	2.02	2.02
Ti	0.00	0.00	0.00	0.00	0.00	0.00	0.01	0.00
Cr	0.00	0.00	0.00	0.00	0.00	0.00	0.00	0.00
Fe	2.10	2.23	2.09	1.82	2.43	2.07	1.73	2.00
Mn	0.10	0.16	0.31	0.57	0.05	0.34	0.91	0.55
Mg	0.61	0.43	0.44	0.49	0.40	0.35	0.21	0.30
Ca	0.11	0.12	0.07	0.09	0.08	0.17	0.10	0.08
Na	0.00	0.00	0.00	0.00	0.00	0.00	0.00	0.00
K	0.00	0.00	0.00	0.00	0.00	0.00	0.00	0.00
Total	7.97	7.98	7.96	7.98	7.98	7.97	7.98	7.97
Alm	0.72 (0.02)	0.76 (0.00)	0.72 (0.01)	0.61 (0.01)	0.82 (0.01)	0.71 (0.00)	0.59 (0.05)	0.68 (0.01)
Pyr	0.21 (0.03)	0.15 (0.01)	0.15 (0.00)	0.16 (0.03)	0.13 (0.01)	0.12 (0.01)	0.07 (0.01)	0.10 (0.00)
Sps	0.04 (0.01)	0.05 (0.01)	0.11 (0.00)	0.19 (0.04)	0.02 (0.00)	0.12 (0.01)	0.31 (0.06)	0.19 (0.00)
Grs	0.04 (0.00)	0.04 (0.01)	0.03 (0.00)	0.03 (0.01)	0.03 (0.00)	0.06 (0.00)	0.03 (0.01)	0.03 (0.00)

Note: All microprobe analyses were performed at the University of California at Los Angeles with a Cameca Camebax electron microprobe. Operating conditions were 15 kV accelerating potential, a 15 nA beam current, and 20 second counting times. A focused (~1 μm) was used for all minerals except plagioclase, for which the beam was defocused to ~5 μm. A ZAF correction algorithm was used with well-characterized natural and synthetic standards. Mineral abbreviations are after Kretz (1983). All oxide data in Table 3 to Table 6 are reported as averages of analyses. Numbers in parentheses after averages give 1σ standard deviation. Calculated mole fractions of mineral components are reported as averages with 1σ standard deviation following in parentheses. Number in parentheses below sample number at top of each column indicates number of analyses averaged.

al., 1994): these are some of the deepest exposures of the Sierra Nevada magmatic arc. P-T conditions in the Japanese Ryoke metamorphic belt are from pelitic thermobarometers (Nakajima, 1994; Okudaira, 1996) and constrain temperatures in the middle crust (10–25 km) of the Cretaceous Eurasian continental arc (e.g., Miyashiro, 1972). The P-T data presented in this study, coupled with other P-T estimates in the Peninsular Ranges batholith from north of the international border (Hill, 1984; Grove, 1986) constrain temperatures from 10 to 25 km.

Granulite and xenolith thermobarometry data were not used to constrain the MBG for several reasons. These include uncertainties regarding geothermal gradients, particularly during the Archean when many granulites formed (e.g., Nutman and Collerson, 1991), the tectonic environment that generated granulite facies metamorphism (e.g., Bohlen, 1991; Brown, 1993), and the environment of xenolith equilibration (e.g., Miller et al., 1992). P-T data are available from granulites and xenoliths from the Mesozoic continental arc exposed in the central and eastern Mojave Desert (e.g., Henry and Dokka, 1992; Miller et al., 1992; and Hanchar et al., 1994). The data were included in Table 8 to illustrate the range of temperature conditions recorded by rocks exhumed from the lower crust of a Mesozoic arc in southwestern North America but were not considered in defining the MBG described below.

TABLE 4. REPRESENTATIVE BIOTITE COMPOSITIONS

(avg. of)	MC294h (4)	CP195 (10)	CT394 (12)	SA7a92 (4)	CB24b92 (11)	SPM294a (14)	SFo594e (10)	LP593b (5)
SiO_2	35.76 (0.11)	35.36 (0.28)	35.80 (0.12)	36.30 (1.14)	34.83 (0.20)	35.80 (0.32)	35.08 (0.57)	35.12 (0.23)
Al_2O_3	17.71 (0.03)	19.57 (0.24)	19.15 (0.24)	18.70 (0.50)	20.00 (0.44)	19.67 (0.26)	19.93 (0.28)	21.14 (0.14)
TiO_2	4.56 (0.01)	3.14 (0.16)	3.61 (0.19)	2.74 (0.19)	2.99 (0.48)	2.36 (0.15)	1.45 (0.20)	1.63 (0.13)
Cr_2O_3	0.03 (0.02)	0.05 (0.03)	0.06 (0.01)	0.05 (0.02)	0.07 (0.04)	0.16 (0.05)	0.05 (0.03)	0.01 (0.02)
FeO	13.63 (0.09)	19.37 (0.54)	18.72 (0.37)	15.57 (0.67)	20.55 (0.62)	18.13 (0.24)	18.38 (0.26)	19.42 (0.51)
MnO	0.04 (0.24)	0.09 (0.04)	0.15 (0.05)	0.45 (0.02)	0.03 (0.03)	0.10 (0.0.)	0.29 (0.07)	0.24 (0.02
MgO	11.89 (0.11)	8.02 (0.26)	8.98 (0.15)	11.12 (0.30)	7.66 (0.44)	8.94 (0.10)	9.54 (0.53)	8.38 (0.20)
CaO	0.00 (0.06)	0.02 (0.01)	0.01 (0.02)	0.02 (0.03)	0.01 (0.01)	0.02 (0.02)	0.05 (0.06)	0.03 (0.02)
Na_2O	0.49 (0.16)	0.16 (0.08)	0.11 (0.04)	0.12 (0.03)	0.33 (0.03)	0.19 (0.02)	0.03 (0.02)	0.05 (0.02)
K_2O	9.01 (0.02)	9.82 (0.16)	9.58 (0.11)	9.80 (0.41)	8.20 (0.22)	8.79 (0.13)	8.73 (0.38)	9.52 (0.21))
Total	93.13 (0.01)	95.61 (0.16)	96.17 (0.48)	94.88 (3.02)	94.66 (0.34)	94.17 (0.66)	93.51 (1.21)	95.53 (0.48)
Sum O	11	11	11	11	11	11	11	11
Si	2.74	2.71	2.69	2.73	2.66	2.74	2.71	2.68
Al	1.60	1.77	1.70	1.66	1.80	1.78	1.81	1.90
Ti	0.26	0.18	0.20	0.15	0.17	0.14	0.08	0.09
Cr	0.00	0.00	0.00	0.00	0.00	0.01	0.00	0.00
Fe	0.87	1.24	1.18	0.98	1.32	1.16	1.19	1.24
Mn	0.00	0.01	0.01	0.03	0.00	0.01	0.02	0.02
Mg	1.36	0.92	1.01	1.25	0.87	1.02	1.10	0.95
Ca	0.00	0.00	0.00	0.00	0.00	0.00	0.00	0.00
Na	0.07	0.02	0.02	0.02	0.05	0.03	0.01	0.01
K	0.88	0.96	0.92	0.94	0.80	0.86	0.86	0.93
Total	7.80 (0.01)	7.81 (0.01)	7.72 (0.01)	7.76 (0.01)	7.68 (0.02)	7.74 (0.02)	7.78 (0.02)	7.83 (0.01)
Al^{iv}	1.26 (0.01)	1.29 (0.01)	1.31 (0.01)	1.27 (0.00)	1.34 (0.01)	1.26 (0.01)	1.29 (0.02)	1.32 (0.01)
Al^{vi}	0.34 (0.01)	0.48 (0.01)	0.39 (0.02)	0.39 (0.02)	0.47 (0.04)	0.52 (0.02)	0.52 (0.02)	0.59 (0.01)
Sum Oct	2.85 (0.01)	2.82 (0.01)	2.79 (0.01)	2.80 (0.01)	2.83 (0.01)	2.85 (0.01)	2.91 (0.03)	2.89 (0.01)
Sum A	0.96 (0.01)	0.99 (0.02)	0.94 (0.01)	0.96 (0.01)	0.85 (0.02)	0.89 (0.01)	0.87 (0.03)	0.94 (0.02)
Fe/Fe+Mg	0.39 (0.01)	0.57 (0.01)	0.54 (0.01)	0.44 (0.00)	0.60 (0.02)	0.53 (0.00)	0.52 (0.02)	0.57 (0.01)
Xmg	0.48 (0.00)	0.32 (0.01)	0.36 (0.01)	0.45 (0.00)	0.31 (0.02)	0.36 (0.00)	0.38 (0.02)	0.33 (0.01)
Xfe	0.31 (0.00)	0.44 (0.01)	0.42 (0.01)	0.35 (0.01)	0.46 (0.01)	0.41 (0.00)	0.41 (0.01)	0.43 (0.01)
Xal	0.12 (0.00)	0.17 (0.00)	0.14 (0.01)	0.14 (0.01)	0.17 (0.01)	0.18 (0.01)	0.18 (0.01)	0.20 (0.00)
Xti	0.09 (0.00)	0.06 (0.00)	0.07 (0.00)	0.06 (0.00)	0.06 (0.01)	0.05 (0.00)	0.03 (0.00)	0.03 (0.00)

THE MAXIMUM BACKGROUND GEOTHERM (MBG)

Figure 4 illustrates the continental arc P-T database and the MBG inferred from it. The MBG is shown as a bold line that traces the locus of minimum contact metamorphic temperature estimates between depths of ~10–25 km. In detail, the MBG traces a geothermal gradient of 40 °C/km from 2 to 10 km, which was based on the heat flow data from active arcs discussed above. Where constrained by metamorphic P-T data from 10 to 25 km, the MBG is ~22 °C/km. This gradient is significantly lower than earlier inferences based on metamorphic P-T data (see Table 1). While the overall geometry of the MBG inferred from petrologic data is similar to the "75% minimum metamorphic gradient" modeled by Barton and Hanson (1989), it is somewhat higher than the 15–18 °C/km minimum metamorphic gradients between 10 and 20 km depths predicted by Barton and Hanson (1989). This is expected because the MBG is inferred from petrologic data and is consistent with the MBG placing an upper limit on ambient temperature conditions during arc magmatism. The scatter of data that record wall-rock temperatures above the MBG is also consistent with the isobaric heating model for low-pressure metamorphism discussed by Barton and Hanson (1989). Numerical models are used in the following section to investigate further the validity of the proposed MBG.

THERMAL MODELING

The difference in temperatures that lie between a shield geotherm and the MBG implies that ambient temperatures in wall

TABLE 5. REPRESENTATIVE PLAGIOCLASE COMPOSITIONS

(avg. of)	MC294h (6)	CP195 (12)	CT394a (10)	SPM294a (7)	SFo594e (11)	LP593b (5)
SiO_2	60.68 (0.58)	58.54 (0.59)	62.43 (0.56)	57.04 (0.75)	63.97 (0.65)	61.92 (0.27)
Al_2O_3	24.81 (0.36)	25.40 (0.41)	24.19 (0.31)	26.89 (0.43)	22.05 (0.70)	24.05 (0.16)
TiO_2	0.01 (0.01)	0.02 (0.02)	0.01 (0.01)	0.03 (0.03)	0.02 (0.012)	0.02 (0.01)
Cr_2O_3	0.01 (0.01)	0.02 (0.02)	0.02 (0.02)	0.02 (0.03)	0.02 (0.02)	0.01 (0.03)
FeO	0.10 (0.06)	0.05 (0.04)	0.02 (0.03)	0.13 (0.03)	0.17 (0.06)	0.03 (0.02)
MnO	0.01 (0.01)	0.02 (0.01)	0.03 (0.02)	0.02 (0.02)	0.03 (0.04)	0.03 (0.02)
MgO	0.00 (0.00)	0.00 (0.00)	0.00 (0.00)	0.00 (0.00)	0.00 (0.02)	0.00 (0.00)
CaO	6.18 (0.65)	7.61 (0.40)	5.18 (0.39)	9.13 (0.31)	3.29 (0.27)	5.16 (0.05)
Na_2O	8.18 (0.32)	7.41 (0.23)	8.80 (0.24)	6.50 (0.29)	9.75 (0.29)	8.84 (0.04)
K_2O	0.19 (0.17)	0.17 (0.03)	0.18 (0.05)	0.06 (0.02)	0.07 (0.02)	0.27 (0.06)
Total	100.17 (0.13)	99.23 (0.55)	100.85 (0.27)	99.81 (0.47)	99.37 (0.65)	100.33 (0.23)
Sum O	8	8	8	8	8	8
Si	2.70	2.64	2.75	2.56	2.84	2.74
Al	1.30	1.35	1.25	1.42	1.15	1.25
Ti						
Cr						
Fe						
Mn						
Mg						
Ca	0.29	0.37	0.24	0.44	0.16	0.24
Na	0.70	0.65	0.75	0.56	0.84	0.75
K	0.01	0.01	0.01	0.00	0.00	0.01
Total	5.01 (0.01)	5.02 (0.01)	5.01 (0.01)	5.01 (0.01)	5.00 (0.03)	5.02 (0.00)
Xan	0.29 (0.03)	0.36 (0.02)	0.24 (0.02)	0.44 (0.02)	0.16 (0.01)	0.24 (0.00)
Xab	0.70 (0.02)	0.63 (0.02)	0.75 (0.02)	0.56 (0.02)	0.84 (0.01)	0.75 (0.00)
Xor	0.01 (0.01)	0.01 (0.00)	0.01 (0.00)	0.00 (0.00)	0.00 (0.00)	0.01 (0.00)

Note: Mineral abbreviations after Kretz (1983).

rocks of the upper and middle crust lie within a narrow envelope during continental arc magmatism. To see if the MBG inferred from petrologic data could develop in the upper and middle crust of a continental arc, we ran two-dimensional heat transfer models that simulate the heating of wall rocks between plutons in the middle crust (5–25 km) and tracked the development of gradients in predicted minimum metamorphic temperatures (PMMT). We also used the models to further investigate whether the MBG represents a reasonable upper boundary for ambient temperature distributions in the middle crust of continental arcs.

Parameterization

Details regarding the numerical approach and parameterization of the simulations are described in the Appendix and Table A1. Sixteen different simulations were run with varying parameters (Table A2). The simulations employ two different initial temperature distributions: linear geothermal gradient of 18°C, which represents a stable shield geotherm, and the MBG described in this study. The use of the MBG as an initial temperature distribution is to test whether the resulting PMMT grossly exceed the temperatures determined via wall-rock thermobarometry and predict widespread crustal melting at unrealistically shallow levels of the crust. The use of a stable shield geotherm is to investigate whether rapid and abundant plutonism will yield PMMT gradients that are reasonably close to the MBG inferred from petrologic data. The models also investigate the effects of variations in the volume and rate of plutonism by simulating wall-rock temperatures between two 20-km-wide plutons. Varying the distance between the two plutons simulates the effects of 50% and 75% pluton volume, which is broadly consistent with mapping from Baja California, México (e.g., Gastil et al., 1975).

The models use two rates of pluton emplacement: simultaneous intrusion and a 5 m.y. difference in the timing of emplacement (hereafter referred to as the simultaneous and differential emplacement models, respectively). Because the characteristic time constant ($t_{char} = L^2/4\kappa$; see Appendix for abbreviations) for a 20-km-wide pluton is <1 m.y., a 5 m.y. difference allows nearly complete cooling after the emplacement of the first pluton. The simultaneous emplacement models have run times of 5 m.y.; the differential emplacement models have 10 m.y. run times. Such time scales are broadly consistent with the geochronology and thermochronology

TABLE 6. REPRESENTATIVE MUSCOVITE AND CORIERITE ANALYSES

	SA7a92 Muscovite		CB24b92 Cordierite
(avg. of)	(8)		(14)
SiO_2	46.54 (0.55)	SiO_2	48.39 (0.24)
Al_2O_3	35.13 (0.29)	Al_2O_3	32.46 (0.24)
TiO_2	0.12 (0.15)	TiO_2	0.01 (0.02)
Cr_2O_3	0.01 (0.01)	Cr_2O_3	0.01 (0.02)
FeO	1.10 (0.13)	FeO	9.45 (0.21)
MnO	0.05 (0.08)	MnO	0.07 (0.02)
MgO	1.07 (0.31)	MgO	7.23 (0.09)
CaO	0.02 (0.02)	CaO	0.01 (0.01)
Na_2O	0.71 (0.19)	Na_2O	0.40 (0.03)
K_2O	10.13 (0.37)	K_2O	0.00 (0.01)
Total	95.18 (0.87)	Total	98.05 (0.52)
Sum O	11	Sum O	18
Si	3.10	Si	5.02
Al	2.76	Al	3.97
Ti	0.01	Ti	0.00
Cr	0.00	Cr	0.00
Fe	0.06	Fe	0.82
Mn	0.00	Mn	0.01
Mg	0.11	Mg	1.12
Ca	0.00	Ca	0.00
Na	0.09	Na	0.08
K	0.89	K	0.00
Total	7.01 (0.01)	Total	11.03 (0.01)
Aliv	0.90 (0.02)	Xfe	0.42 (0.01)
Alvi	1.85 (0.02)	Xmg	0.58 (0.01)
Sum A	0.98 (0.01)		
Xal	0.91 (0.01)		
Xk	0.90 (0.03)		
Xna	0.09 (0.03)		

of the eastern Peninsular Ranges batholith and track the high-temperature portion of the wall rocks' thermal history.

Results

Table A2 summarizes the results from the modeling. Figure 5 shows isotherms from three simulations that varied the volume and rate of plutonism. The region of interest in the simulations lies between the plutons because this most closely simulates wall rocks between nested plutons. Monitoring gradients in the predicted minimum metamorphic temperatures at different depths allows comparison with the MBG recorded by wall-rock thermobarometry as described above. Figure 5 shows the geometry of gradients in the PMMT. In cases of simultaneous emplacement of 50% and 75% plutons, gradients in PMMT are vertical and located midway between the plutons (Figs. 5A and 5B). For models that simulate differential timing of emplacement, the PMMT gradients are subvertical and displaced slightly toward the second pluton emplaced during the simulation (Fig. 5C). Because the simulations in this study emplace plutons between depths of 5–25 km, the results of the modeling are not relevant for crustal levels deeper than 25 km.

The sensitivity of the simulation results varies with different parameters. The assumption of a uniform magmatic emplacement temperature versus pressure-dependent temperatures dictated by the tonalite solidus produces a negligible effect on the PMMT. Increasing the volume of plutons from 50% to 75% has a strong effect and increases the predicted temperatures at a given structural level by ~50–75 °C (Fig. 6A). Changing the rate of plutonism from simultaneous to differential emplacement increases temperatures by a similar amount (Fig. 6B). The sensitivity of the simulations to the volume and rate of plutonism does not change significantly with the higher initial temperature distribution dictated by the MBG, which suggests it represents a reasonable initial temperature distribution.

The geometry of the PMMT gradients is sensitive to the initial temperature distribution. Models that employ the linear 18°C/km geothermal gradient predict minimum metamorphic temperature gradients that are ~10–20 °C/km lower than models that use the MBG as an initial temperature distribution. The linear geotherm models start at lower temperatures, so the PMMT gradients from this initial condition show greater curvature than the models that use the MBG as an initial condition (Fig. 6A). The mid-crustal (10–25 km) PMMT gradients from the MBG models (20–22 °C/km) are higher than the 15 °C/km temperature gradients from 10 to 30 km predicted by Barton and Hanson (1989), who used a background thermal gradient of ~22 °C/km.

Numerical simulations that employ an initial geothermal gradient of 18 °C/km yield PMMT gradients that nearly coincide with the MBG from 10 to 20 km depths when a high volume of plutons are emplaced rapidly (Fig. 6C). Because numerical simulations that use a stable shield geotherm as an initial condition yield PMMT gradients that are close to the petrologic MBG only when magmatism is most voluminous and rapid, the results suggest the MBG is a reasonable constraint on the maximum background temperatures during arc magmatism. Numerical simulations that employ the MBG as the initial temperature distribution yield PMMT that fall below the wet tonalite solidus from 0 to 20 km and above the solidus at greater depths (Fig. 6A). This result also supports the validity of the MBG, as the use of this temperature distribution as an initial condition does not predict widespread partial melting of the upper crust during the rapid emplacement of a high volume of plutons. The result is also broadly consistent with the observation of migmatites in mid-crustal wall rocks (>20 km) in much of the eastern Peninsular Ranges batholith in Baja California, México (e.g., Rothstein, 1997). Taken together, the results of the numerical modeling suggest that the MBG inferred from petrologic data effectively brackets the upper end of maximum ambient wall-rock temperatures in the middle crust of an active arc. In the following section, we discuss the implications of this geotherm for seismic velocity, structural, and thermochronologic studies in these terranes.

TABLE 7. THERMOBAROMETRY RESULTS

Sample	Locality*	Latitude Longitude	Reaction†	P (kbar) (±1σ)	T (°C)§ (±1σ)
MC294h	Sierra Cucapah (100)	N32°32' W115°38.7'	GASP	4.0 (0.65)	575 (8)
CP195	Cantu Palms (250)	N32°21.22' W115°49.74'	GASP	4.6 (0.47)	720 (25)
CT394a	Cañon Tajo (300)	N32°15.7' W115°49'	GASP	4.7 (0.50)	676 (10)
SA7a92	Sierra Abandonada (350)	N31°3.2' W114°52.8'	SGAM	5.0 (0.04)	614 (7)
CB24b92	Cañade El Baroso (50)	N30°48.8' W115°13.7'	CASBGQ	5.8 (0.07)	668 (37)
SPM294a	Agua Caliente (75)	N30°37.56' W115°16.1'	GASP	4.1 (0.18)	610 (6)
SFo594e	Sierra San Francisquito (500)	N29°37.46' W114°16.1'	GASP	3.2 (0.54)	476 (18)
LP593b	Los Paredones (500)	N28°39.1' W113°23.9'	GASP	3.1 (0.26)	590 (18)

*Number beneath locality denotes distance, in meters, of sample from pluton–wall rock contact.
†Reactions are as follows (mineral abbreviations after Kretz, 1983):
GASP: 3 pl = grs + 2 sil + qtz
SGAM: alm + ms = ann + sil + qtz
pyr + ms + ann + 2 sil + qtz
CASBGQ: 2 pyr + 5 qtz + 4 sil = 3 crd
2 ann + 3 crd = 4 sil + 5 qtz + 2 phl + 2 alm
§All temperatures were calculated from the garnet-biotite Fe-Mg exchange reaction: alm + phl = pyr + ann

DISCUSSION

Relatively low (~22 °C/km) geothermal gradients in the middle crust of continental arcs are an important consideration in modeling tectonism from seismic velocity. Because seismic velocities decrease with increasing temperature (Griffin and O'Reilly, 1987; Weaver and Tarney, 1984; Stüwe and Sandiford, 1994), the background geotherm is important in the interpretation of the broad structure and composition of the crust in continental arcs. The inferred position of the Mohorovicic (Moho) discontinuity will depend on the geothermal gradient at the time such velocities are measured. Cooler geothermal gradients in continental arcs will also yield estimates of more intermediate compositions for the lower crust from seismic data (Griffin and O'Reilly, 1987) that are consistent with petrologic models and the composition of granulite terranes.

The geothermal gradient described in this study is also relevant to the mechanical evolution of continental arcs. Low geothermal gradients accelerate cooling and diminish the length scales of thermal "softening" or weakening around crystallizing plutons in the shallow and middle crust (Lister and Baldwin, 1993). This accentuates the pulses of multiple, short-lived deformation events in heavily intruded regions that are inferred from numerical investigations and combined structural, geochronologic, and thermochronologic studies (e.g., Sandiford et al., 1991; Paterson and Tobisch, 1992; Stüwe et al., 1993; Lister and Baldwin, 1993;

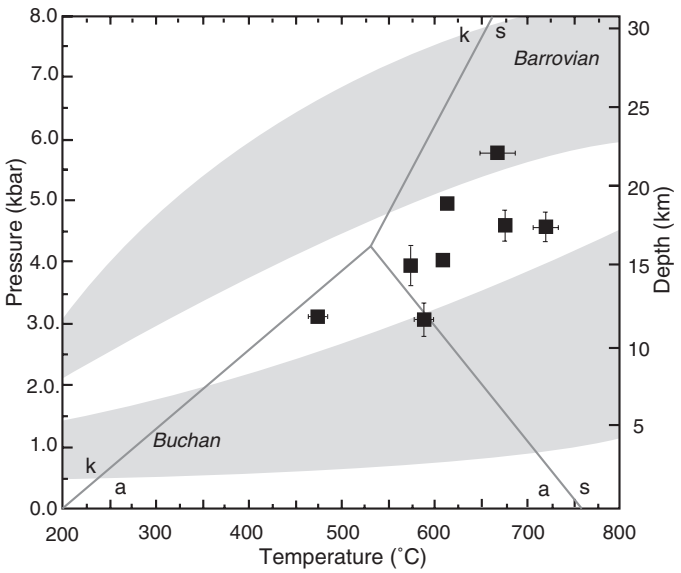

Figure 3. P-T diagram of thermobarometry estimates from eastern Peninsular Ranges batholith presented in this study. Error bars of 1σ are shown where estimates are not smaller than size of symbol. Aluminum silicate stability fields taken from Bohlen et al. (1991). Buchan and Barrovian P-T fields after Turner (1981).

TABLE 8. P-T CONSTRAINTS FROM CONTINENTAL MAGMATIC ARCS

Location	Data	P-T constraints	Source
Andes Mountains Bolivia	prospecting boreholes	25–57 °C/km	Giese (1994)
Bolivia and Peru	mineral and petroleum exploration holes	20–35 °C/km	Henry and Pollack (1988)
Peninsular Ranges Mount San Jacinto	pelitic/calc-silicate phase relations/thermobarometry	620–800 °C, 3.2–3.4 kb	Hill (1984)
Santa Rosa Mountains	pelitic and calc-silicate phase relations	650–800 °C, 2.0–4 .0 kb	Erskine (1986)
Box Canyon	pelitic phase relations and thermobarometry	650–700 °C, 4.0–5.0 kb	Grove (1993; 1994)
Sierra Nevada Tehachapi Mountains	pelitic phase relations and thermobarometry	680–770 °C, 5.3–6.0 kb	Dixon et al. (1994)
Lake Isabella	pelitic phase relations and thermobarometry	620–720 °C, 5.5–6.0 kb	Dixon et al. (1994)
Ritter Range	calc-silicate phase relations	>450–500 °C, 1.8–2.3 kb	Hanson et al. (1993)
Hope Valley	calc-silicate phase relations and thermobarometry	440–540 °C, 1.8–2.3 kb	Ferry (1989)
Twin Lakes	calc-silicate phase relations and thermobarometry	600–650 °C, 2.5–3.5 kb	Davis and Ferry (1993)
Mount Morrison	calc-silicate phase relations	500–600 °C, 2.5–3.0 kb	Morgan (1975)
Mount Tallac	metavolcanic phase relations	625–650 °C,1.8–2.0 kb	Loomis (1966)
Cascade Mountains Washington	water wells and mineral and geothermal exploration holes	45 °C/km	Blackwell et al. (1990)
Northern Oregon	water wells and geothermal exploration holes	65 °C/km	Blackwell et al. (1982)
Japan Ryoke Belt	pelitic phase relations and thermobarometry	650–700 °C, 3.5–4.0 kb	Nakajima (1994)
Ryoke Belt	pelitic phase relations and thermobarometry	460–590 °C, 2.5–3.5 kb 630–690 °C, 3.0–5.0 kb 730–770 °C, 5.5–6.5 kb	Okudaira (1996)
Granulites scattered locations	thermobarometry	750–850 °C, 6.5–8.5 kb	Bohlen (1991)
Mojave Desert Eastern Mojave Xenoliths Waterman Complex	phase relationships and thermobarometry	 750 °C, 11 kb 750–800 °C, 10–12 kb	 Hanchar et al. (1994) Henry and Dokka (1992)

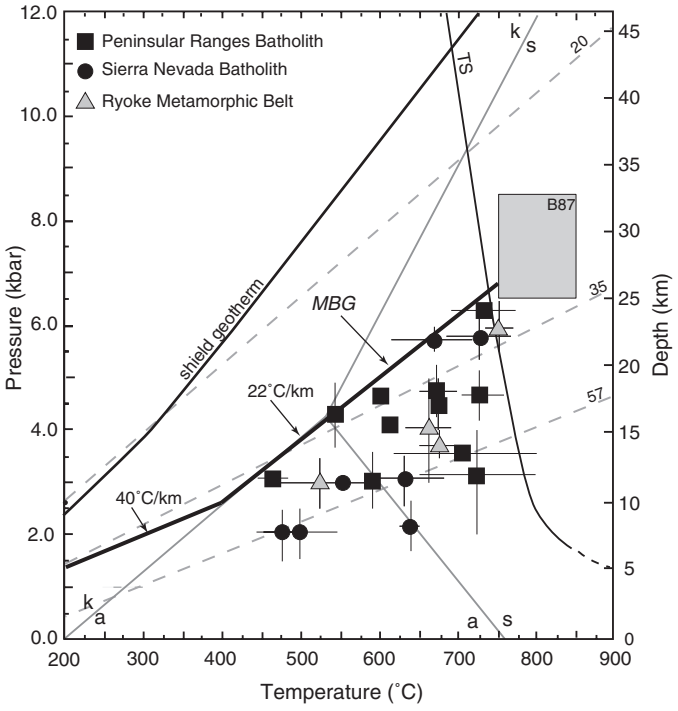

Figure 4. Summary P-T diagram showing available P-T estimates from Table 8 used to constrain maximum background geotherm (MBG). Aluminosilicate stability fields from Bohlen et al. (1991), stable shield geotherm from Morgan (1984), and vapor-saturated tonalite solidus (TS) from Johannes (1984) are shown for reference. Large gray box labeled *B87* encloses mean granulite P-T conditions from Bohlen (1987); other symbols are explained in diagram. Dashed gray lines labeled 20, 35, and 57 delineate linear geothermal gradients of 20 °C/km, 35 °C/km, and 57 °C/km extrapolated from heat flow data in active arcs (see Table 2). For clarity, thermobarometry symbols denote mean P-T estimates summarized in Table 8. Error bars are taken from reported studies when available or are arbitrarily set at ±50 °C and 0.5 kbar. Symbols with no error bars have reported errors that are smaller than size of the symbol. Black dashed line labeled MBG represents maximum background geotherm inferred from P-T data. Where constrained by P-T data from 10 to 30 km, locus of minimum temperatures in array defines a gradient of ~22 °C/km. Assumption of a 40 °C/km gradient from 0 to 10 km is consistent with available P-T constraints and studies summarized in Table 1.

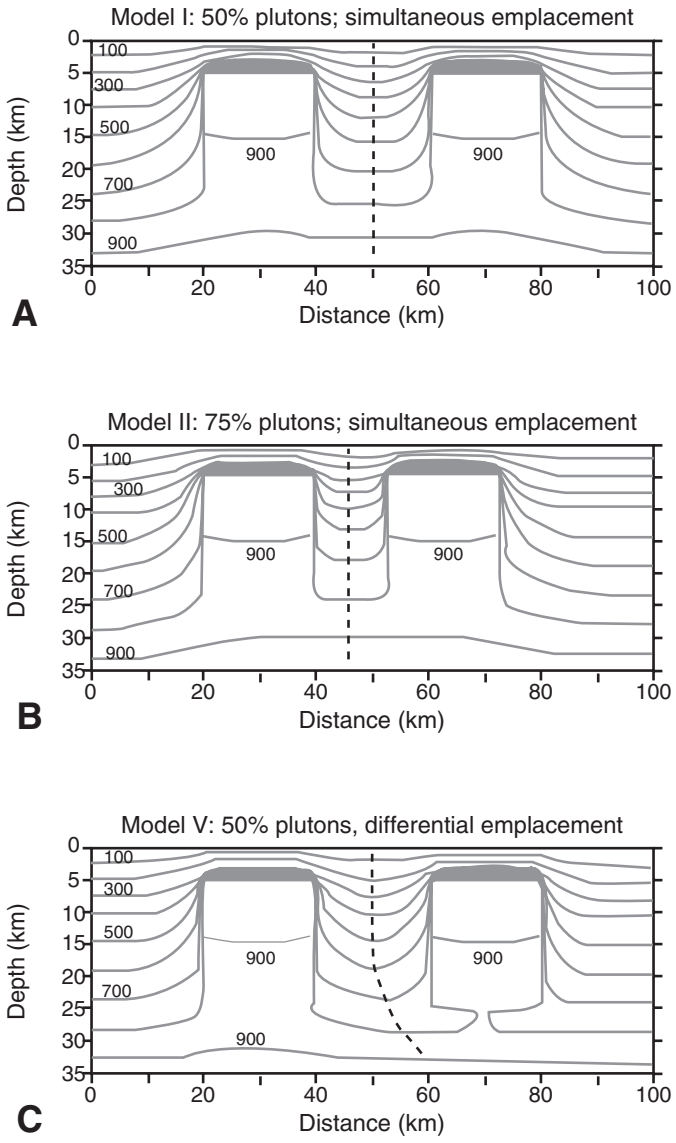

Figure 5. Examples of thermal modeling grids. Grid measures 100 km across and 40 km deep. Plutons are 20 km wide and 20 km tall and are emplaced instantaneously between depths of 5 and 25 km. Solid gray lines labeled 100–900 in 200 °C increments are isotherms showing distribution of maximum temperatures recorded in each simulation. Dashed black lines trace locus of minimum temperatures recorded from surface to 35 km depths and represent gradients in predicted minimum metamorphic temperatures (PMMT). A: Maximum temperature distribution for model I with 50% pluton volume and simultaneous rate of emplacement; PMMT is vertical and located midway between plutons. B: Maximum temperature distribution for model II with 75% pluton volume and simultaneous rate of emplacement. PMMT is vertical and located midway between plutons, which are more closely spaced to simulate 75% pluton volume. C: Maximum temperature distribution for model V with 50% pluton volume and 5 m.y. time lag between emplacement of plutons. PMMT is sub-vertical and displaced toward second pluton. See appendix for details regarding parameterization of each model (indicated by roman numeral).

Karlstrom et al., 1993). Because this structural setting will consist of domains of high strain rates localized around cooling plutons, their spatial and temporal distribution will be discontinuous. However, over the duration of arc emplacement, these domains may coalesce to form broad belts of deformation that appear continuous in the geologic record (e.g., Patterson and Tobisch, 1992).

The recognition of low geothermal gradients in batholiths also affects modeling denudation histories from thermochronologic data. Assuming high mid-crustal geothermal gradients in arc terranes will lead to underestimating the rate of unroofing recorded by various mineral thermochronometers. Low temperature (~450 °C) $^{40}Ar/^{39}Ar$ mica and K-feldspar and fission-track apparent ages from rocks in arc terranes such as the Peninsular Ranges batholith are typically on the order of 5–10 m.y. younger than pluton emplacement ages recorded by zircon U-Pb systematics. Because thermal anomalies from mid-crustal magma sources will likely decay over 5–10 m.y. toward low (~20 °C/km) pre-magmatic temperatures, it may be inappropriate to use geothermal gradients inferred from short-lived peak temperatures recorded in contact metamorphic mineral assemblages to interpret exhumation processes that operate over longer time scales.

CONCLUSION

Metamorphic data from the eastern Peninsular Ranges batholith in Baja California, México, provide constraints on the distribution of wall-rock temperatures in a continental magmatic arc characterized by a relatively simple thermal history. Combining these data with P-T data from similar terranes results in the recognition of a maximum background geotherm characterized by a significant change from ~40 °C/km in the upper crust (0–10 km) to ~22 °C/km in the middle crust (10–25 °C/km). This mid-crustal geotherm is significantly lower than the 35–50 °C/km gradients previously inferred from low-pressure metamorphic P-T data and is somewhat higher than 15–18 °C/km gradients in the middle crust inferred from previous modeling studies. Recognition of this geothermal gradient may lower estimates of the depth to the seismic Moho and increase strain and unroofing rates inferred from structural and thermochronologic studies, respectively.

APPENDIX

The numerical approach uses the explicit finite-difference method to approximate the analytical solution to the heat flow equation in two dimensions:

$$\frac{dT}{dt} = \kappa\left(\frac{\partial^2 T}{\partial x^2} + \frac{\partial^2 T}{\partial z^2} + \frac{A}{K}\right)$$

where κ is the thermal diffusivity ($m^2\ s^{-1}$), T is temperature (°C), t is time (s), x is the horizontal Cartesian coordinate (m), z is the depth and increases downward (m), A is the radiogenic heat production (mW m^{-3}), and k is the thermal conductivity (mW m^{-1} $°C^{-1}$). The numerical code for these simulations was written

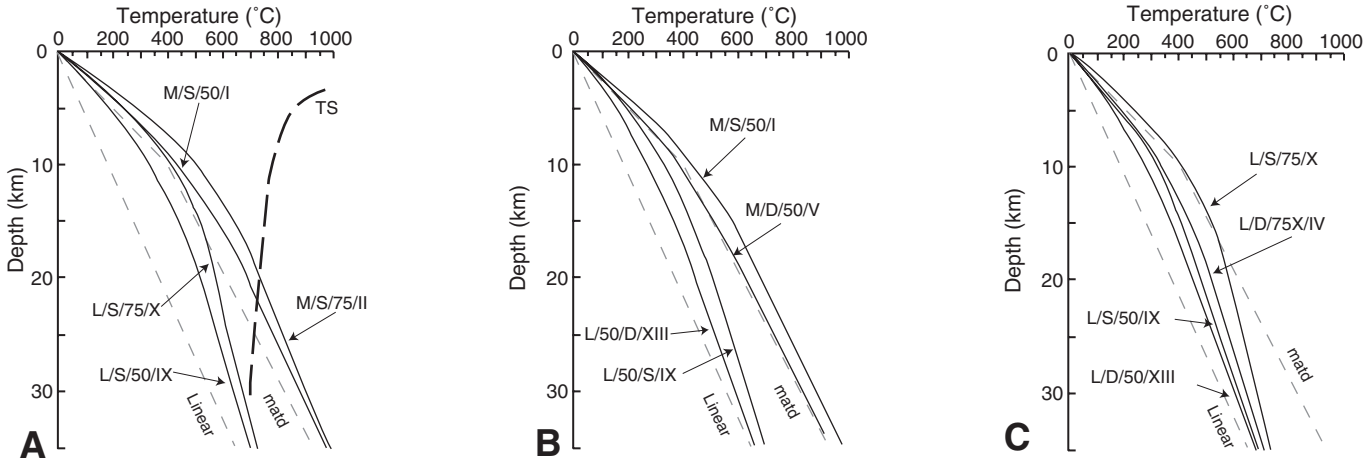

Figure 6. Comparison of gradients in predicted minimum metamorphic temperatures (PMMT). Abbreviations refer to following initial conditions for thermal models: L—18 °C/km initial temperature distribution; M— maximum background geotherm (MBG) initial temperature distribution; D—differential emplacement (5 m.y. between plutons); S—Simultaneous emplacement; 50—50% pluton volume; 75—75% pluton volume. Roman numerals correspond to simulations described in Table A2. A: Comparison of simultaneous intrusion models that illustrate sensitivity of PMMT to pluton volume. TS indicates wet tonalite solidus (Johannes, 1984). B: Comparison of 50% pluton volume models that illustrate sensitivity of PMMT to simultaneous versus differential pluton emplacement. C: Comparison of various simulations using 18 °C/km linear ambient geotherm. Most rapid and highest volume of plutonism yields a gradient in PMMT that is broadly similar to MBG described in this study. See text for further discussion.

by Hanson and Barton (1989) but was modified to allow implementation of different initial temperature distributions. Although implicit methods exhibit greater numerical stability (Carnahan et al., 1969; Harrison and Clarke, 1979), the explicit finite-difference method facilitates the adjustment of thermal parameters after each time step to better simulate the thermal effects of the latent heat of crystallization, which require consideration to accurately model temperatures near intrusive contacts (Jaeger, 1964).

The numerical code was compared with an implicit finite-difference code written by O.M. Lovera to test the stability and convergence of the explicit finite-difference method and the accuracy of the results. For the simple case of wall rock heating from the crystallization of a single pluton, the numerical approaches are indistinguishable from each other. The Hanson and Barton code facilitates the simulation of varying combinations of pluton volume and timing of intrusions. The code uses a nine-point approximation of the second derivative of temperature in the heat flow equation to improve numerical stability and convergence (Hanson and Barton, 1989).

The finite difference grid consists of a two-dimensional array of equally spaced points. The spacing between points was 1 km, such that the grid measured 100 km wide and 40 km deep (Fig. 6). Each simulation involves the instantaneous emplacement of two 20-km-wide plutons between depths of 5 and 25 km in each simulation. Instantaneous emplacement yields lower temperatures than for cases of forceful emplacement, a preheated ascent path, or if extension facilitates intrusion.

The models use one of two temperature distributions for the tonalitic plutons. One set of models assumes uniform emplacement temperatures of 900 °C throughout the 20-km-thick magma chamber. The other set of models uses experimental constraints on the wet tonalite solidus (Johannes, 1984) to dictate depth-dependent variations in emplacement temperatures. Averaging the supersolidus temperatures in magma chambers after each time step simulates the thermal effects of convection; this approximation maximizes heat flow from the intrusions and tends to overestimate temperatures near the pluton contact. While temperatures are above the solidus, halving the thermal diffusivity inside the magma chamber simulates the thermal effects of the latent heat of crystallization (see Table A1). The thermal effects of this approximation diminish rapidly from the pluton contact and are negligible at distances greater than one-quarter of the width of the pluton. The effect of the latent heat of crystallization is calculated over a 100 °C temperature interval between emplacement and solidus temperatures.

The thermal effects of metamorphic and melting reactions are ignored because it is unclear that uniformly adjusting the wall-rock thermal diffusivity over a particular temperature interval appropriately simulates the thermal effects of the discontinuous and continuous metamorphic reactions that occur within a crust that has a heterogeneous bulk composition. Because this study is most concerned with gradients in temperature rather than absolute values, this simplification had a negligible effect on our interpretation of the model results.

The models also ignore alternative heat sources for low-pressure metamorphism. Because the Peninsular Ranges batholith lacks large-scale regional metasomatic zones, the models do not consider the regional effects of heat transport by migrating

TABLE A1. PARAMETERIZATION OF THERMAL MODELS

Parameter/Symbol	Definition/Value
MBG	Maximum ambient temperature distribution 40 °C/km (0–10 km); 22 °C/km (10–35 km)
Linear Geotherm	Linear geothermal gradient. 18 °C/km
K	Thermal conductivity
κ_m	Thermal diffusivity, supersolidus. 5.0 x 10^{-7} cm^2 s^{-1}
κ_r	Thermal diffusivity, solidified pluton and country rocks. 1.0 x 10^{-6} cm^2 s^{-1}
T_s	Solidus temperature. 1000 °C, 5–10 km; 920 °C, 10–15 km; 860 °C, 15–20 km; 820 °C, 20–25 km
T_o	Surface temperature. 0 °C
T	Initial temperature at depth z.
Δt	Time step increment. 10,000 years.
ΔX	Spacing between nodes in x-direction. 1000 m (100 km wide grid)
ΔZ	Spacing between nodes in z-direction. 1000 m (40 km deep grid)
A	Internal heat production at depth z.

TABLE A2. THERMAL MODELING INITIAL CONDITIONS AND RESULTS

Model	Initial Temperature	Pluton Temperature	Pluton Volume	Timing	PMMT
I	MBG	Tonalite Solidus	50%	Simultaneous	44 °C/km 0–10 km 22 °C/km 10–35 km
II	MBG	Tonalite Solidus	75%	Simultaneous	50 °C/km 0–10 km 20 °C/km 10–35 km
III	MBG	Uniform (900 °C)	50%	Simultaneous	44 °C/km 0–10 km 22 °C/km 10–35 km
IV	MBG	Uniform (900 °C)	75%	Simultaneous	50 °C/km 0–10 km 20 °C/km 10–35 km
V	MBG	Tonalite Solidus	50%	Differential	40 °C/km 0–10 km 22 °C/km 10–35 km
VI	MBG	Tonalite Solidus	75%	Differential	41 °C/km 0–10 km 22 °C/km 10–35 km
VII	MBG	Uniform (900 °C)	50%	Differential	40 °C/km 0–10 km 22 °C/km 10–35 km
VIII	MBG	Uniform (900 °C)	75%	Differential	41 °C/km 0–10 km 22 °C/km 10–35 km
IX	Linear	Tonalite Solidus	50%	Simultaneous	33 °C/km 0–10 km 16 °C/km 10–35 km
X	Linear	Tonalite Solidus	75%	Simultaneous	41 °C/km 0–10 km 13 °C/km 10–35 km
XI	Linear	Uniform (900 °C)	50%	Simultaneous	33 °C/km 0–10 km 16 °C/km 10–35 km
XII	Linear	Uniform (900 °C)	75%	Simultaneous	41 °C/km 0–10 km 13 °C/km 10–35 km
XIII	Linear	Tonalite Solidus	50%	Differential	27 °C/km 0–10 km 16 °C/km 10–35 km
XIV	Linear	Tonalite Solidus	75%	Differential	32 °C/km 0–10 km 15 °C/km 10–35 km
XV	Linear	Uniform (900 °C)	50%	Differential	27 °C/km 0–10 km 16 °C/km 10–35 km
XVI	Linear	Uniform (900 °C)	75%	Differential	31 °C/km 0–10 km 15 °C/km 10–35 km

Note: Linear geotherm is 18 °C/km; the MBG is 40 °C from 0–10 km and 22 °C/km from 10–30 km as defined in the text. Simultaneous and differential timing of pluton emplacement are explained in the text. PMMT—predicted minimum metamorphic temperature; MBG—Maximum backgroud geotherm.

low-density metamorphic fluids (e.g., Hoisch, 1987; Hanson, 1995). The models did not investigate the consequences of magmatic underplating, which may be important in the generation of granulites at depths >35 km in batholiths. Because the geologic, petrologic, geochronologic, and thermochronologic frameworks of the batholith suggest that Cretaceous plutonism dominated the thermal evolution of the Peninsular Ranges batholith, the thermal models focused on this aspect of the metamorphic evolution of the batholith.

Numerous crustal models and combinations of the physical and thermal properties of rocks allow the calculation of the ~18 °C/km geotherm used in the linear geotherm models in this study (e.g., Turcotte and Schubert, 1982). An example of parameters that yield an ~18°C/km geotherm for a one-layer, 35-km-thick crust with a homogenous distribution of radioactive elements includes internal heat production (A) = 0.7 mW/m^3; basal heat flux (Q*) = 25 W/m^2; thermal conductivity (k) = 2.5 $W\ m^{-1}\ °C^{-1}$.

ACKNOWLEDGMENTS

This work benefited from our association with M. Grove, O. Lovera, R. Jones, and R. Alkaly at the University of California at Los Angeles and through discussions with G. Gastil, V. Todd, D. Kimbrough, J. Lee, and J. Stock on various aspects of field geology in the eastern batholith and from reviews by J. Fletcher and D. Whitney. This research was in part supported by National Science Foundation grant EAR 94-05999 (C.M.) and grants from Sigma Xi and the California chapter of the American Mineralogical Society (D.R.).

REFERENCES CITED

Arndt, J., Bartel, T., Scheuber, E., and Schuilling, F., 1997, Thermal and rheological properties of granodioritic rocks from the central Andes, north Chile: Tectonophysics, v. 271, p. 75–88.

Barton, M.D., and Hanson, R.B., 1989, Magmatism and the development of low-pressure metamorphic belts: implications from the western United States and thermal modeling: Geological Society of America Bulletin, v. 101, p. 1051–1065.

Barton, M.D., Battles, D.A., Bebout, G.A., Capo, R.C., Christensen, J.N., Davis, S.R., Hanson, R.B., Michelsen, C.J., and Trim, H.E., 1988, Mesozoic contact metamorphism in the western United States, *in* Ernst, W.G., ed., Metamorphism and crustal evolution of the western conterminous United States, Rubey Volume VII: Englewood Cliffs, N.J., Prentice-Hall, p. 110–178.

Berman, R.G., 1990, Mixing properties of Ca-Mg-Fe-Mn garnets: American Mineralogist, v. 75, p. 328–344.

Berman, R.G., 1991, Thermobarometry using multi-equilibrium calculations: A new technique, with petrological applications: Canadian Mineralogist, v. 29, p. 833–855.

Birch, F., 1961, The velocity of compressional waves in rocks to 10 kbar: Journal of Geophysical Research, v. 66, p. 2199–2224.

Blackwell, D.D., Bowen, R.G., Hull, D.A., Riccio, J., and Steele, J.L., 1982, Heat flow, arc volcanism, and subduction in northern Oregon: Journal of Geophysical Research, v. 87, p. 8735–8754.

Blackwell, D.D., Steele, J.L., Kelley, S., and Korosec, M.A., 1990, Heat flow in the state of Washington and thermal conditions in the Cascade Range: Journal of Geophysical Research, v. 95, p. 19,495–19,516.

Bodorokos, S., Sandiford, M., Oliver, N.H.S., and Cawood, P.A., 2002, High-T, low-P metamorphism in the paleoproterozoic Halls Creek orogen, northern Australia: The middle crustal response to a mantle-related transient thermal pulse: Journal of Metamorphic Geology, v. 20, p. 217–237.

Bohlen, S.R., 1991, On the formation of granulites: Journal of Metamorphic Geology, v. 9, p. 223–229.

Bohlen, S.R., Montana, A., and Kerrick, D.M., 1991, Precise determinations of the equilibria kyanite = sillimanite and kyanite = andalusite and a revised triple point for Al_2SiO_5 polymorphs: American Mineralogist, v. 76, p. 677–680.

Brown, M., 1993, P-T-t evolution of orogenic belts and the causes of regional metamorphism: Journal of the Geological Society of London, v. 150, p. 227–241.

Carnahan, B., Luther, H.A., and Wilkes, J.O., 1969, Applied numerical methods: New York, John Wiley & Sons, 603 p.

Christensen, N.I., 1982, Seismic velocities, *in* Carmichael, R.S., ed., Handbook of physical properties of rocks, V. 2: Boca Raton, Florida, CRC Press, p. 1–228.

Christensen, N.I., and Fountain, D.M., 1975, Constitution of the lower continental crust based on experimental studies of seismic velocities in granulite: Geological Society of America Bulletin, v. 86, p. 227–236.

Crawford, M.L., Hollister, L.S., and Woodsworth, G.J., 1987, Crustal deformation and regional metamorphism across a terrane boundary, Coast Plutonic Complex, British Columbia: Tectonics, v. 6, p. 343–361.

Davis, S.R., and Ferry, J.M., 1993, Fluid infiltration during contact metamorphism of interbedded marble and calc-silicate hornfels, Twin Lakes area, central Sierra Nevada, California: Journal of Metamorphic Geology, v. 11, p. 71–88.

De Yoreo, J.J., Lux, D.R., and Guidotti, C.V., 1989, The role of crustal anatexis and magma migration in the thermal evolution of regions of thickened continental crust, *in* Daly, J.S., Cliff, R.A., and Yardley, B.W.D., ed., Evolution of metamorphic belts: Geological Society [London] Special Publication 42, p. 187–202.

De Yoreo, J.J., Lux, D.R., and Guidotti, C.V., 1991, Thermal modeling in low-pressure/high-temperature metamorphic belts: Tectonophysics, v. 188, p. 209–238.

Dixon, E.T., Essene, E.J., and Halliday, A.N., 1994, Critical tests of hornblende barometry, Lake Isabella to Tehachapi area, southern Sierra Nevada, California [abs.]: Eos (Transactions, American Geophysical Union), v. 74, p. 744.

Dokka, R.K., 1984, Fission-track geochronologic evidence for Late Cretaceous mylonitization and Early Paleocene uplift of the northeastern Peninsular Ranges, California: Geophysical Research Letters, v. 11, p. 46–49.

England, P.C., and Richardson, S.W., 1977, The influence of erosion upon the mineral facies of rocks from different metamorphic environments: Journal of the Geological Society of London, v. 134, p. 201–213.

England, P.C., and Thompson, A.B., 1984, Pressure-temperature-time paths of regional metamorphism I. Heat transfer during the evolution of regions of thickened continental crust: Journal of Petrology, v. 25, p. 894–928.

Erskine, B.G., 1986, Mylonitic deformation and associated low-angle faulting of the northern Peninsular Ranges batholith, southern California [Ph.D. dissertation thesis]: Berkeley, University of California.

Erskine, B.G., and Wenk, H.R., 1985, Evidence for Late Cretaceous crustal thinning in the Santa Rosa mylonite zone, southern California: Geology, v. 13, p. 274–277.

Ferry, J.M., 1989, Contact metamorphism of roof pendants at Hope Valley, Alpine County, California, USA: Contributions to Mineralogy and Petrology, v. 101, p. 402–417.

Fuhrman, M.L., and Lindsley, D.H., 1988, Ternary-feldspar modeling and thermometry: American Mineralogist, v. 73, p. 201–215.

Furlong, K.P., and Fountain, D.M., 1986, Continental crustal underplating: Thermal considerations and seismic-petrologic consequences: Journal of Geophysical Research, v. 91, p. 8285–8294.

Furlong, K.P., Hanson, R.B., and Bowers, J.R., 1991, Modeling thermal regimes, *in* Kerrick, D.A., ed., Contact metamorphism: Reviews in Mineralogy, v. 26, p. 437–505.

Furukawa, Y., and Uyeda, S., 1989, Thermal state under Tohoku arc with consideration of crustal heat generation: Tectonophysics, v. 164, p. 175–187.

Gastil, R.G., and Miller, R.H., 1993, The prebatholithic stratigraphy of peninsular California: Boulder, Colorado, Geological Society of America Special Paper 279, 163 p.

Gastil, R.G., Philips, R.P., and Allison, E.C., 1975, Reconnaissance geology of the state of Baja California: Boulder, Colorado, Geological Society of America Memoir 140, 170 p.

George, P.G., and Dokka, R.K., 1994, Major Late Cretaceous cooling events in the eastern Peninsular Ranges, California, and their implications for Cordilleran tectonics: Geological Society of America Bulletin, v. 106, p. 903–914.

Giese, P., 1994, Geothermal structure of the central Andean crust-implications for heat transport and rheology, *in* Reutter, K.J., Scheuber, E., and Wigger,

P.J., eds., Tectonics of the southern central Andes; structure and evolution of an active continental margin: Berlin, Springer-Verlag, p. 69–76.
Gill, J., 1981, Orogenic andesites and plate tectonics: Berlin, Springer, 390 p.
Goodwin, L.B., and Renne, P.R., 1991, Effects of progressive mylonitization on Ar retention in biotites from the Santa Rosa mylonite zone, California, and thermochronologic implications: Contributions to Mineralogy and Petrology, v. 108, p. 283–297.
Griffin, W.L., and O'Reilly, S.Y., 1987, Is the continental Moho the crust-mantle boundary?: Geology, v. 15, p. 241–244.
Grissom, G.C., DeBari, S.M., Page, S.P., Page, R.F.N., Villar, L.M., Coleman, R.G., and de Ramirez, M.V., 1991, The deep crust of an early Paleozoic arc; the Sierra de Riambalá, northwestern Argentina, *in* Harmon, R.S., and Rapela, C.W., eds., Andean magmatism and its tectonic setting: Boulder, Colorado, Geological Society of America Special Paper 265, p. 189–200.
Grove, M., 1986, Metamorphism of the Box Canyon area, Peninsular Ranges batholith, San Diego County, California [M.S. thesis]: Los Angeles, University of California, 174 p.
Grove, M., 1993, Thermal histories of southern California basement terranes [Ph.D. thesis]: Los Angeles, University of California, 419 p.
Grove, M., 1994, Contrasting denudation histories within the east-central Peninsular Ranges batholith (33°N): Geological Society of America Cordilleran Section Field Trip Guidebook, p. 235–240.
Hanchar, J.M., Miller, C.F., Wooden, J.L., Bennett, V.C., and Staude, J.M.G., 1994, Evidence from xenoliths for a dynamic lower crust, eastern Mojave Desert, California: Journal of Petrology, v. 35, p. 1377–1415.
Hanson, B.N., and Gast, P.W., 1967, Kinetic studies in contact metamorphic zones: Geochimica et Cosmochimica Acta, v. 31, p. 1119–1153.
Hanson, R.B., 1995, The hydrodynamics of contact metamorphism: Geological Society of America Bulletin, v. 107, p. 595–611.
Hanson, R.B., and Barton, M.D., 1989, Thermal development of low-pressure metamorphic belts: Results from two-dimensional numerical models: Journal of Geophysical Research, v. 94, p. 10,363–10,377.
Hanson, R.B., Sorensen, S.S., Barton, M.D., and Fiske, R.S., 1993, Long-term evolution of fluid-rock interactions in magmatic arcs: Evidence from the Ritter Range pendant, Sierra Nevada, California, and numerical modeling: Journal of Petrology, v. 34, p. 23–62.
Harrison, T.M., and Clarke, G.K.C., 1979, A model of the thermal effects of igneous intrusion and uplift as applied to Quottoon pluton, British Columbia: Canadian Journal of Earth Sciences, v. 16, p. 411–420.
Henry, D.J., and Dokka, R.K., 1992, Metamorphic evolution of exhumed middle to lower crustal rocks in the Mojave Extensional Belt, southern California: Journal of Metamorphic Geology, v. 10, p. 347–364.
Henry, S.G., and Pollack, H.N., 1988, Terrestrial heat flow above the Andean subduction zone in Bolivia and Peru: Journal of Geophysical Research, v. 93, p. 15,153–15,162.
Hill, R.I., 1984, Petrology and petrogenesis of batholithic rocks, San Jacinto Mountains, southern California [Ph.D.] dissertation: Pasadena, California, California Institute of Technology, 660 p.
Hoisch, T.D., 1987, Heat transport by fluids during Late Cretaceous regional metamorphism in the Big Maria mountains, southeastern California: Geological Society of America Bulletin, v. 98, p. 549–553.
Hyndman, D.W., and Foster, D.A., 1989, Plutonism at deep crustal levels: The Idaho batholith, Montana and Idaho, *in* Hyndman, D.W., Rutland, C., and Hardyman, R.F., eds., Cordilleran volcanism, plutonism, and magma generation at various crustal levels, Montana and Idaho: Washington, D.C., American Geophysical Union, p. 3–15.
Ingebritsen, S.E., Sherrod, D.R., and Mariner, R.H., 1989, Heat flow and hydrothermal circulation in the Cascade Range, north-central Oregon: Science, v. 243, p. 1458–1462.
Ingebritsen, S.E., Sherrod, D.R., and Mariner, R.H., 1992, Rates and patterns of groundwater flow in the Cascade range volcanic arc, and the effect of subsurface temperatures: Journal of Geophysical Research, v. 97, p. 4599–4627.
Jaeger, J.C., 1964, Thermal effects of intrusions: Reviews in Geophysics, v. 2, p. 433–466.
Joesten, R., and Fisher, G., 1988, Kinetics of diffusion-controlled mineral growth in the Christmas Mountains (Texas) contact aureole: Geological Society of America Bulletin, v. 100, p. 714–732.
Johannes, W., 1984, Beginning of melting in the granite system Qz-Or-Ab-An-H_2O: Contributions to Mineralogy and Petrology, v. 86, p. 264–273.
Johnson, S.E., Tate, M.C., and Fanning, C.M., 1999, New geologic mapping and SHRIMP U-Pb zircon data in the Peninsular Ranges batholith, Baja California, México: Evidence for a suture?: Geology, v. 27, p. 743–746.
Karlstrom, K.E., Miller, C.F., Kingsbury, J.A., and Wooden, J.L., 1993, Pluton emplacement along an active ductile thrust zone, Piute Mountains, southeastern California: Interactions between deformational and solidification processes: Geological Society of America Bulletin, v. 105, p. 213–230.
Kohn, M.J., and Spear, F.S., 1991, Error propagation for barometers: 2. Application to rocks: American Mineralogist, v. 76, p. 138–147.
Kohn, M.J., Spear, F.J., Harrison, T.M., and Dalziel, I.W.D., 1995, $^{40}Ar/^{39}Ar$ geochronology and P-T-t paths from the Cordillera Darwin metamorphic complex, Tierra del Fuego, Chile: Journal of Metamorphic Geology, v. 13, p. 251–270.
Kretz, R., 1983, Symbols for rock-forming minerals: American Mineralogist, v. 68, p. 277–279.
Krumenacher, D., Gastil, R.G., Bushee, J., and Doupont, J., 1975, K-Ar apparent ages, Peninsular Ranges batholith, southern California and Baja California: Geological Society of America Bulletin, v. 86, p. 760–768.
Lister, G.S., and Baldwin, S.L., 1993, Plutonism and the origin of metamorphic core complexes: Geology, v. 21, p. 607–610.
Loomis, A.A., 1966, Contact metamorphic reactions and processes in the Mt. Tallac roof remnant, Sierra Nevada, California: Journal of Petrology, v. 7, p. 221–245.
Lovera, O.M., Grove, M., Kimbrough, D.L., and Abbott, P.L., 1999, A method for evaluating basement exhumation histories from closure age distributions of detrital minerals: Journal of Geophysical Research, v. 104, no. B2, p. 29,419–29,438.
Lovering, T.S., 1935, Theory of heat conduction applied to geological problems: Geological Society of America Bulletin, v. 48, p. 69–94.
Lucassen, F., and Franz, G., 1996, Magmatic arc metamorphism: Petrology and temperature history of metabolic rocks in the coastal Cordillera of northern Chile: Journal of Metamorphic Geology, v. 14, p. 249–265.
Lux, D.R., De Yoreo, J.J., Guidotti, C.V., and Decker, E.R., 1985, Role of plutonism in low-pressure metamorphic belt formation: Nature, v. 323, p. 794–797.
Mahon, K.I., Harrison, T.M., and Drew, D.A., 1988, Ascent of a granitoid diapir in a temperature-varying medium: Journal of Geophysical Research, v. 93, p. 1174–1188.
McDougall, I., and Harrison, T.M., 1988, Geochronology and Thermochronology by the $^{40}Ar/^{39}Ar$ Method: Oxford, Oxford University Press, 212 p.
McMullin, D.W.A., Berman, R.G., and Greenwood, H.J., 1991, Calibration of the SGAM thermobarometer for pelitic rocks using data from phase-equilibrium experiments and natural assemblages: Canadian Mineralogist, v. 29, p. 889–908.
Miller, C.F., Watson, E.B., and Harrison, T.M., 1988, Perspectives on the source, segregation, and transport of granitoid magmas: Transactions of the Royal Society of Edinburgh, Earth Sciences, v. 79, p. 135–156.
Miller, C.F., Hanchar, J.M., Wooden, J.L., Bennet, V.C., Harrison, T.M., Wark, D.A., and Foster, D.A., 1992, Source region of a granite batholith: Evidence from lower crustal xenoliths and inherited accessory minerals: Transactions of the Royal Society of Edinburgh, Earth Sciences, v. 83, p. 49–62.
Minch, J.A., 1979, The Late Mesozoic–Early Tertiary framework of continental sedimentation, northern Peninsular Ranges, Baja California, México, *in* Abbott, P.L., ed., Eocene depositional systems, San Diego, California: Los Angeles, Society of Economic Paleontologists and Mineralogists Pacific Section, p. 43–67.
Miyashiro, A., 1972, Metamorphism and related magmatism in plate tectonics: American Journal of Science, v. 272, p. 629–656.
Miyashiro, A., 1973, Metamorphism and metamorphic belts: New York, Wiley, 492 p.
Morgan, B.A., 1975, Mineralogy and origin of skarns in the Mount Morrison pendant, Sierra Nevada, California: American Journal of Science, v. 275, p. 119–142.
Morgan, P., 1984, The thermal structure and thermal evolution of the continental lithosphere, *in* Pollack, H.N., ed., Structure and evolution of the continental lithosphere: Physics and Chemistry of the Earth, v. 15, p. 107–193.
Nakajima, T., 1994, The Ryoke plutonometamorphic belt: Crustal section of the Cretaceous Eurasian continental margin: Lithos, v. 33, p. 51–66.
Norton, D.L., 1984, Theory of hydrothermal systems: Annual Reviews of Earth and Planetary Sciences, v. 12, p. 155–177.
Nutman, A.P., and Collerson, K.D., 1991, Very early Archean crustal-accretion complexes preserved in the North Atlantic craton: Geology, v. 19, p. 791–794.
Okudaira, T., 1996, Temperature-time path for the low-pressure Ryoke metamorphism, Japan, based on chemical zoning in garnet: Journal of Metamorphic Geology, v. 14, p. 427–440.

Ortega-Rivera, M.A., Farrar, E., Hanes, J.A., Archibald, D.A., Gastil, R.G., Kimbrough, D.L., Zentilli, M., Lopez Martinez, M., Feraud, G., and Ruffet, G., 1997, Chronological constraints on the thermal and tilting history of the Sierra San Pedro Martir pluton, Baja California, México, from U/Pb, $^{40}Ar/^{39}Ar$, and fission-track geochronology: Geological Society of America Bulletin, v. 109, p. 728–745.

Paterson, S.R., and Tobisch, O.T., 1992, Rates of processes in magmatic arcs: Implications for the timing and nature of pluton emplacement and wall rock deformation: Journal of Structural Geology, v. 14, p. 291–300.

Rothstein, D.A., 1997, Metamorphism and denudation of the eastern Peninsular Ranges batholith, Baja California, México [Ph.D. dissertation]: Los Angeles, University of California, 445 p.

Rothstein, D.A., and Hoisch, T.D., 1994, Multiple intrusions and low-pressure metamorphism in the central Old Woman Mountains, south-eastern California: Constraints from thermal modelling: Journal of Metamorphic Geology, v. 12, p. 723–734.

Rothstein, D.A., Manning, C.E., and Grove, M., 1994, Denudation patterns in the eastern Peninsular Ranges batholith, Baja California, México [abs.]: Eos (Transactions, American Geophysical Union), v. 75, p. 229.

Rothstein, D.A., Grove, M., and Manning, C.E., 1995, Role of the main gulf escarpment in the denudation of the east-central Peninsular Ranges batholith, Baja California, México: Insights from high resolution $^{40}Ar/^{39}Ar$ thermochronology [abs.]: Eos (Transactions, American Geophysical Union), v. 76, p. 639.

Rusmore, M.E., and Woodsworth, G.J., 1994, Evolution of the eastern Waddington thrust belt and its relation to the mid-Cretaceous Coast Mountains arc, western British Columbia: Tectonics, v. 13, p. 1052–1067.

Sandiford, M., Martin, N., Zhou, S., and Graser, G., 1991, Mechanical consequences of granite emplacement during high-T, low-P metamorphism and the origin of "anticlockwise" PT paths: Earth and Planetary Science Letters, v. 107, p. 164–172.

Schilling, F.R., and Parzsch, G.M., 2001, Quantifying partial melt fraction in the crust beneath the central Andes and the Tibetan plateau: Physics and Chemistry of the Earth, Part A, v. 26, p. 239–246.

Sharp, R.V., 1967, San Jacinto fault zone in the Peninsular Ranges of southern California: Geological Society of America Bulletin, v. 78, p. 706–729.

Silver, L.T., and Chappell, B.W., 1988, The Peninsular Ranges batholith: An insight into the evolution of the Cordilleran batholiths of southwestern North America: Transactions of the Royal Society of Edinburgh; Earth Sciences, v. 79, p. 105–121.

Simpson, C., 1984, Borrego Springs–Santa Rosa mylonite zone: A Late Cretaceous west-directed thrust in southern California: Geology, v. 12, p. 8–11.

Springer, M., and Förster, A., 1998, Heat-flow density across the central Andean subduction zone: Tectonophysics, v. 291, p. 123–139.

Stock, J.M., and Hodges, K.V., 1989, Pre-Pliocene extension around the Gulf of California and the transfer of Baja California to the Pacific Plate: Tectonics, v. 8, p. 99–115.

Stüwe, K., and Sandiford, M., 1994, Contribution of deviatoric stresses to metamorphic P-T paths: An example appropriate to low-P, high-T metamorphism: Journal of Metamorphic Geology, v. 12, p. 445–454.

Stüwe, K., Sandiford, M., and Powell, R., 1993, Episodic metamorphism and deformation in low-pressure, high-temperature terranes: Geology, v. 21, p. 829–832.

Taylor, H.P., 1986, Igneous rocks: II. Isotopic case studies of Circum-Pacific magmatism, *in* Valley, J.W., Taylor, H.P., and O'Neil, J.R., eds., Stable isotopes in high temperature geological processes: Reviews in Mineralogy, v. 16, p. 273–318.

Thomson, C.N., and Girty, G.H., 1994, Early Cretaceous intra-arc ductile strain in Triassic-Jurassic and Cretaceous continental margin arc rocks, Peninsular Ranges, California: Tectonics, v. 13, p. 1108–1119.

Thompson, R.N., 1972, Melting behavior of two Snake River lavas at pressures up to 35 kb: Carnegie Institution of Washington Yearbook, v. 71, p. 406–410.

Todd, V.R., Erskine, B.G., and Morton, D.M., 1988, Metamorphic and tectonic evolution of the northern Peninsular Ranges batholith, southern California, *in* Ernst, W.G., ed., Metamorphism and crustal evolution of the western United States (Rubey Volume VII): Englewood Cliffs, N.J., Prentice-Hall, p. 894–937.

Todd, V.R., Girty, G.H., Shaw, W.E., and Jachens, R.C., 1991, Geochemical, geochronologic, and structural characteristics of Jurassic plutonic rocks, Peninsular Ranges, California [abs]: Geological Society of America Abstracts with Programs, v. 23, p. A249.

Turcotte, D.L., and Schubert, G., 1982, Geodynamics: Applications of continuum physics to geological problems: New York, John Wiley and Sons, 450 p.

Turner, F.J., 1981, Metamorphic petrology: Mineralogical, field, and tectonic aspects: New York, McGraw-Hill, 524 p.

Uyeda, W., and Watanabee, T., 1982, Terrestrial heat flow in western South America: Tectonophysics, v. 83, p. 63–70.

Walawender, M.J., Gastil, R.G., Clinkenbeard, J.P., McCormick, W.V., Eastman, B.G., Wernicke, F.S., Wardlaw, M.S., Gunn, S.H., and Smith, B.M., 1990, Origin and evolution of the zoned La Posta-type plutons, eastern Peninsular Ranges batholith, southern and Baja California, *in* Anderson, J.L., ed., The nature and origin of Cordilleran magmatism: Boulder, Colorado, Geological Society of America Memoir 174, p. 1–18.

Weaver, B.L., and Tarney, J., 1984, Empirical approach to estimating the composition of the continental crust: Nature, v. 310, p. 575–577.

Wells, P.R.A., 1980, Thermal models for the magmatic accretion and subsequent metamorphism of continental crust: Earth and Planetary Science Letters, v. 46, p. 253–265.

Wickham, S.R., and Oxburgh, E.R., 1985, Continental rifts as a setting for regional metamorphism: Nature, v. 318, p. 330–333.

Wickham, S.R., and Oxburgh, E.R., 1987, Low-pressure regional metamorphism in the Pyrenees and its implications for the thermal evolution of rifted continental crust: Philosophical Transactions of the Royal Society of London, v. 321A, p. 219–242.

Wiswall, C.G., and Hyndman, D.W., 1987, Emplacement of the main plutons of the Bitterroot lobe of the Idaho batholith, *in* Vallier, T.L., and Brooks, H.C., eds., Geology of the Blue Mountains Region of Oregon, Idaho, and Washington: The Idaho batholith and its border zone: U.S. Geological Survey Professional Paper 1436, p. 59–72.

Wyllie, P.J., 1979, Petrogenesis and the physics of the earth, *in* Yoder, H.S., ed., The evolution of the igneous rocks: Fiftieth anniversary perspectives: Princeton, Princeton University Press, p. 483–520.

Yoder, H.S., Jr., and Tilley, C.E., 1962, Origin of basalt magmas: An experimental study of natural and synthetic rock systems: Journal of Petrology, v. 3, p. 342–532.

Manuscript Accepted by the Society June 2, 2003

Printed in the USA